IEEE Access
Multidisciplinary ⋮ Rapid Review ⋮ Open Access Journal

Received March 8, 2022, accepted May 8, 2022, date of publication May 16, 2022, date of current version May 31, 2022.

Digital Object Identifier 10.1109/ACCESS.2022.3175164

Carrier-Based Aircraft Precision Landing Using Direct Lift Control Based on Incremental Nonlinear Dynamic Inversion

FEI LUO[1], JUNHONG ZHANG[1,2], PENGFEI LYU[1], ZHENGBAO LIU[2], (Member, IEEE), AND WEI TANG[3], (Member, IEEE)

[1]First Aircraft Design and Research Institute, Aviation Industry Corporation of China, Xi'an 100022, China
[2]School of Civil Aviation, Northwestern Polytechnical University, Xi'an 710072, China
[3]School of Automation, Northwestern Polytechnical University, Xi'an 710072, China

Corresponding author: Fei Luo (15624950251@163.com)

(Fei Luo and Junhong Zhang are co-first authors.)

This work was supported by the Control Law Design Office, Flight Control System Institute, First Aircraft Design and Research Institute of Aviation Industry Corporation of China, Ltd.

ABSTRACT Conventional direct lift control (DLC) design in carrier landing is not accepted by pilots since it is not fully decoupled and has heavy control burden. Nevertheless, when using dynamic inversion, developed in recent years as the baseline control framework, the control architecture can dynamically decouple control state channels and simplify control logic. In this study, the incremental dynamic inversion control (INDI) method is used to realize the DLC of the carrier-based aircraft precision landing control law and compare the dynamic inversion control (NDI). Meanwhile, the robustness of the INDI control framework is analyzed. A landing simulation system is completed to verify that using the NDI/INDI+DLC framework can fully exploit and reflect the advantage of DLC in carrier landing. The results show that the proposed NDI/INDI+DLC, i.e., the precision landing control architecture, can use the rapidity of DLC to correct minor errors of landing and improve landing accuracy quickly. At the same time, decoupling of DLC based on INDI can also reduce the complexity of the landing operation and improve the landing success rate.

INDEX TERMS Carrier aircraft landing, control engineering, nonlinear control systems, tracking loops, trajectory optimization.

I. INTRODUCTION

Attempts to explore direct lift for improving the landing quality of carrier-based aircraft can be traced back to sixty years ago [1]. In 1965, an F-8C crusader airplane was flight-tested by the Naval Air Test Center. Pilots used a direct lift thumbwheel and trim control wheel installed on the stick to realize direct lift control (DLC), which was implemented with a horizontal-tail-to-aileron-loop interconnector. The results of the F-8C demonstration program then formed the baseline design for DLC of the F-14A Tomcat during its design and development [2]. However, a limitation of the early DLC design was that it required independent control input thumbwheel; although it could improve the landing quality to a certain degree, pilots rarely used lift thumbwheel due to other heavy maneuvering tasks in the last twenty seconds of the landing stage. For nearly thirty years, it was indicated that the design method of DLC in the F14 was a kind of a ''chicken rib'' [3]. The main reason is that this kind of DLC required control surfaces used for statically trimming pitch moment disturbances induced by DLC function; commonly, a pre-compensator generated required trim surface deflections. Although the gains and feedback states were elaborately chosen, the results of this method only achieved partial direct lift effects while needed more DLC thumbwheel inputs. Recently, Lockheed Martin proposed a new integrated DLC method for X-35C carrier aircraft. The benefits of integrating DLC into the baseline control strategy without additional cockpit inceptors were confirmed [4]. Based on the DLC design foundation of X-35C, the precision landing control (PLC) project of F/A-18E/F and F-35C, disclosed in 2016 by the U.S. Navy, was developed [3]. PLC was intimately referred to as a ''magic carpet'' by carrier-based aircraft pilots.

The associate editor coordinating the review of this manuscript and approving it for publication was Engang Tian.

The development of DLC used in carrier landing projects enlightens this paper to consider decoupling control logic complexity as important as using DLC to improve the landing accuracy. In order to achieve the goals mentioned above, the dynamic inversion control architecture, which is different from traditional classical control theory, is applied as the baseline control framework for direct lift control. Especially, nonlinear dynamic inversion (NDI) is a popular paradigm of the flight control law in recent years. Moreover, the dynamic inversion control method has been used in various aircrafts, such as passenger aircraft [5], helicopters [6], rotorcraft [7], VTOL transition aircraft [8], [9], numerous kinds of UAVs [10]–[14], and even some flexible aircraft [15], [16]. Additionally, there are many dynamic inversion control schemes of automatic carrier landing systems (ACLSs) for reference or as lessons [17]–[20]. However, dynamic inversion control is only used mostly in the attitude loop. There are few references on dynamic inversion with direct lift control to improve flight trajectory tracking performance. The main reason is that the trajectory dynamics equation of the aircraft cannot be directly written as an affine nonlinear system that is easy to design for dynamic inversion control like the attitude dynamics equation. However, there are still attempts to use direct lift control in dynamic inversion control to obtain desired flight performance. Reference [21] presented the benefits of adding direct lift control capabilities to a UAV within an INDI control framework. The simulation results indicated that direct lift improves the control performance projected to wind disturbances. However, the control object is a fixed-wing UAV with rotors that generate direct lift at low speed. That is different from carrier-based aircraft that use flaps to generate direct lift at high speed. In Reference [22], a novel integrated control design with dynamic control allocation was proposed to tackle the challenges of DLC-based control for small fixed-wing UAVs. This paper inspired the author to study a more suitable DLC control allocation algorithm based on NDI/INDI in the future. The most similar idea with this paper is the one in Reference [23]. Lombaerts *et al.* described how DLC was incorporated into a nonlinear auto-flight control algorithm and accurate flight path tracking under atmospheric disturbances. Nevertheless, the critical problem of DLC decoupling was not considered. Consequently, DLC was only used as a compensation strategy to reject wind disturbances. In other words, the direct lift control mode for carrier landing was not fully achieved.

Therefore, this paper proposes a precision landing control scheme with DLC based on NDI/INDI as the baseline control. This is different from conventional DLC design methodology, which is difficult to fully explore advantage of direct lift and achieve direct lift control mode. Using NDI/INDI as the baseline control law of carrier precision landing can dynamically decouple attitude control from trajectory tracking, which meets the requirements of dynamic decoupling for DLC.

Compared to other related studies [21]–[23], the main contributions of this study can be summarized as follows:

TABLE 1. The basic parameters of fix wing carrier aircraft.

Parameters	Value	Parameters	Value
Length	17.60m	Landing angle of attack	8.22°
Wingspan	24.56m	Control actuators frequency bandwidth	60Hz
Height	5.58m	Flight height	0~114m
Empty weight	18.3t	Landing gear position	down
Landing speed	191km/h	Wing area	60.9m^2
Flaperon range	0~20°	Trailing flaps range	0~40°

(1) To achieve the dynamical decoupling effect of attitude stabilization and trajectory tracking with DLC, a practical DLC framework is proposed for carrier landing based on the baseline control law of NDI/INDI. The new DLC implemented in the NDI/INDI control scheme quietly meets the requirements of carrier precision landing with the ability of disturbance rejection, and the control-logic complexity is significantly reduced in the control design stage.

(2) Different from most dynamic inversion control implemented in the attitude loop only, this paper attempted to design two separate and parallel dynamic inversion control loops for the attitude and trajectory according to the aircraft dynamic characteristics of long-period mode and short-period mode. In this way, the DLC+NDI/INDI control framework is adequate to reflect direct lift standouts for improving landing performance in practice.

This paper is organized as follows: Section II describes the physical and mathematical model of the landing control system. Section III presents a brief interpretation of the DLC+NDI/INDI framework. Section IV implements the precision control law in the DLC+NDI/INDI architecture. The numerical simulation results are illustrated and discussed in Section V. Section VI draws main conclusions.

II. LANDING SYSTEM DESCRIPTION

In this section, the landing control system consist of carrier aircraft parameters and model, aerodynamics forces and moments, ship air wake and sensors and actuators will be elaborated described.

A. CARRIER AIRCRAFT PARAMETERS

The control object is a fixed-wing carrier-based aircraft, and the basic parameters of carrier-based aircraft are provided in Table 1. Fig. 1 demonstrates fundamental outlook and shape, especially the deployment and location of control surfaces. The direct lift control consists of two trailing edge flaps and two flaperons.

B. AIRCRAFT MODEL EQUATIONS

The aircraft dynamics equation is a 6-DOF rigid body dynamics equation. The left side of the equation includes aerodynamic force, engine thrust, and gravity. The specific dynamics equation is as follows:

$$\dot{\boldsymbol{V}} = m^{-1}[\boldsymbol{F}_{\mathrm{A}}(\boldsymbol{x},\boldsymbol{u},\boldsymbol{d}) + \boldsymbol{F}_{\mathrm{T}}(\boldsymbol{x},\boldsymbol{u})] - \boldsymbol{\omega} \times \boldsymbol{V} + \boldsymbol{T}_{\mathrm{be}}[\,0 \quad 0 \quad g]^{\mathrm{T}}$$

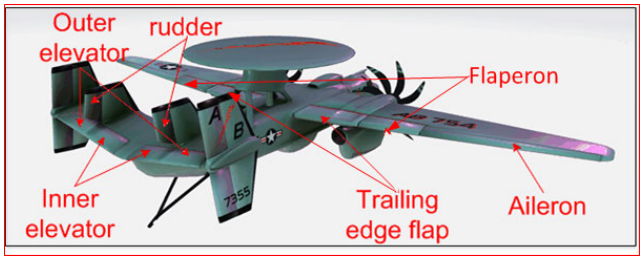

FIGURE 1. The outlook of controlled carrier-based aircraft.

$$\dot{\boldsymbol{\omega}} = \boldsymbol{J}(\boldsymbol{d})^{-1}\left[\boldsymbol{M}_{\mathrm{A}}(\boldsymbol{x},\boldsymbol{u},\boldsymbol{d}) + \boldsymbol{M}_{\mathrm{T}}(\boldsymbol{x},\boldsymbol{u}) - \boldsymbol{\omega}\times\boldsymbol{J}(\boldsymbol{d})\boldsymbol{\omega}\right] \quad (1)$$

where $\boldsymbol{V} = [\,u\ v\ w\,]^{\mathrm{T}}$ is speed in the body frame. $\boldsymbol{\omega} = [\,p\ q\ r\,]^{\mathrm{T}}$ is three-axis angular rate in the body frame. $\boldsymbol{F}_{\mathrm{A}}, \boldsymbol{M}_{\mathrm{A}}$ represent aerodynamic force and moment, and $\boldsymbol{F}_{\mathrm{T}}, \boldsymbol{M}_{\mathrm{T}}$ respectively represent engine thrust and moment produced by the thrust to the center of gravity. $\boldsymbol{x}, \boldsymbol{u}, \boldsymbol{d}$ respectively represent aircraft control state, control input, and model uncertainty parameter. $\boldsymbol{T}_{\mathrm{be}}$ represents coordinate transformation matrix of ground inertial coordinate to the aircraft body. g is gravity constant. m is aircraft weight. $\boldsymbol{J}$ represents the moment matrix of aircraft inertia:

$$\boldsymbol{J}(p) = \begin{bmatrix} J_{\mathrm{xx}} & 0 & -J_{\mathrm{xz}} \\ 0 & J_{\mathrm{yy}} & 0 \\ -J_{\mathrm{xz}} & 0 & J_{\mathrm{zz}} \end{bmatrix} \quad (2)$$

Generally, the Euler angle is used to represent the body angular motion of aircraft. The body coordinate is coincident with the ground coordinate after coordinate rotation in three fixed orders. In this process, three Euler angles are generated, and the relationship between three body frame angular rates and the Euler angular rates are as follows:

$$\begin{bmatrix} \dot{\phi} \\ \dot{\theta} \\ \dot{\psi} \end{bmatrix} = \begin{bmatrix} 1 & \sin\phi\tan\theta & \cos\phi\tan\theta \\ 0 & \cos\phi & -\sin\phi \\ 0 & \sin\phi/\cos\theta & \cos\phi/\cos\theta \end{bmatrix} \begin{bmatrix} \dot{p} \\ \dot{q} \\ \dot{r} \end{bmatrix} \quad (3)$$

Since the landing mission is only a part of the overall flight envelope of carrier-based aircraft, the attitude control is switched back through the stick command range design during takeoff. When the angular motion is represented by Euler angle, the singular problem is not avoided. Thus, the angular kinematics equation is usually expressed by quaternion method, and the specific kinematics equations are as follows:

$$\begin{aligned} \dot{\boldsymbol{R}} &= \boldsymbol{L}_{\mathrm{eb}}\boldsymbol{V} \\ \dot{\boldsymbol{q}} &= \frac{1}{2}\boldsymbol{E}(\boldsymbol{q})\,\boldsymbol{\omega} \end{aligned} \quad (4)$$

where $\boldsymbol{R} = \left[\,x\ y\ h\,\right]^{\mathrm{T}}$ represents the displacement to the center of gravity line and $\boldsymbol{L}_{\mathrm{eb}}$ represents the coordinate transformation matrix of the body frame to the ground frame. And $\boldsymbol{q} = \left[\,q_0\ q_1\ q_2\ q_3\,\right]^{\mathrm{T}} = \left[\,q_0\ \boldsymbol{q}_{\mathrm{v}}^{\mathrm{T}}\,\right]^{\mathrm{T}}$. Among them:

$$\boldsymbol{E}(\boldsymbol{q}) = \begin{pmatrix} -\boldsymbol{q}_{\mathrm{v}}^{\mathrm{T}} \\ -\boldsymbol{s}\left(\boldsymbol{q}_{\mathrm{v}}\right) + q_0\boldsymbol{I}_{3\times 3} \end{pmatrix},$$

$$\boldsymbol{s}\left(\boldsymbol{q}_{\mathrm{v}}\right) = \begin{bmatrix} 0 & q_3 & -q_2 \\ -q_3 & 0 & q_1 \\ q_2 & -q_1 & 0 \end{bmatrix} \quad (5)$$

In the control loop and aerodynamic calculation modules, quaternion is used to transfer back to Euler angle as follows:

$$\boldsymbol{\Phi} = \begin{pmatrix} \phi \\ \theta \\ \psi \end{pmatrix} = \begin{pmatrix} \arctan_2\left[2\left(q_0q_1 + q_2q_3\right), \left(1 - q_1^2 - q_2^2\right)\right] \\ \arcsin\left[2\left(q_0q_2 - q_1q_3\right)\right] \\ \arctan_2\left[2\left(q_0q_3 + q_1q_2\right), \left(1 - q_2^2 - q_3^2\right)\right] \end{pmatrix} \quad (6)$$

C. AERODYNAMIC FORCE AND MOMENT

The aerodynamic force and moment are calculated by the defined aerodynamic coefficients in stability coordinate frame as follows:

$$\begin{aligned} \boldsymbol{F}_{\mathrm{A}}^{\mathrm{s,cg}}(\boldsymbol{x},\boldsymbol{u},\boldsymbol{p}) &= \frac{1}{2}\rho V_{\mathrm{tas}}^2 S \begin{bmatrix} -C_D \\ C_Y \\ C_L \end{bmatrix}, \\ \boldsymbol{M}_{\mathrm{A}}^{\mathrm{s,cg}}(\boldsymbol{x},\boldsymbol{u},\boldsymbol{p}) &= \frac{1}{2}\rho V_{\mathrm{tas}}^2 S \begin{bmatrix} bC_{\mathrm{l}} \\ cC_{\mathrm{m}} \\ bC_{\mathrm{n}} \end{bmatrix} \end{aligned} \quad (7)$$

Specifically, the aerodynamic coefficients of the aircraft are obtained by the wind tunnel test data. It is calculated according to the specific components of force and moment coefficients. Taking the pitching moment coefficient as an example:

$$\begin{aligned} Cm = {} & Cm_{\mathrm{base}} + dCm_{\mathrm{base\_Tc}} + Cm_{\mathrm{Lat}} + dCm_{\mathrm{Lg\_Lon}} \\ & + dCm_{\mathrm{Lg\_Tc}} + dCm_{\mathrm{Lg\_Lat}} + dCm_{\mathrm{De}} + dCm_{\mathrm{Da}} \\ & + dCm_{\mathrm{Dr}} + dCm_{\mathrm{q}} + dCm_{\mathrm{da}} + dCm_{\mathrm{ground\_lon}} \\ & + dCm_{\mathrm{ground\_lat}} \end{aligned} \quad (8)$$

It is clear that the data components of aerodynamic coefficient are mainly divided by the basic quantity (Cm_{base}) and related with pull coefficient ($dCm_{\mathrm{base\_Tc}}$), slipstream effect (Cm_{Lat}), lateral and longitudinal ground effect ($dCm_{\mathrm{Lg\_Lat}}$, $dCm_{\mathrm{Lg\_Lon}}$), landing gear effect related with pull coefficient ($dCm_{\mathrm{Lg\_Tc}}$), aerodynamic rudder surface effect (dCm_{De}), aerodynamic aileron surface effect (dCm_{Da}), aerodynamic rudder surface effect (dCm_{Dr}), induced quantity (dCm_{q}), attack angle effect (dCm_{da}), longitudinal and lateral ground effect ($dCm_{\mathrm{ground\_lon}}$, $dCm_{\mathrm{ground\_lat}}$). In this way, the aerodynamic model is built from Look-Up tables data with polynomial interpolation method.

In terms of the direct lift control surfaces, this fixed-wing carrier aircraft uses trailing edge flaps. The natural position of trailing edge flaps is trimmed at 30 (down) degrees. The flaps can leave the central location with a maximum value of ± 10 degrees. Fig. 2 indicates the difference of aerodynamic lift changed by direct lift surface deflection or attack of angle.

The other source of force and moment is engine thrust $\boldsymbol{F}_{\mathrm{T}}$ and moment $\boldsymbol{M}_{\mathrm{T}}$. The simulation model uses the characteristic data provided by the engine manufacturer to establish the Look-Up table to build the simulation model of the engine.

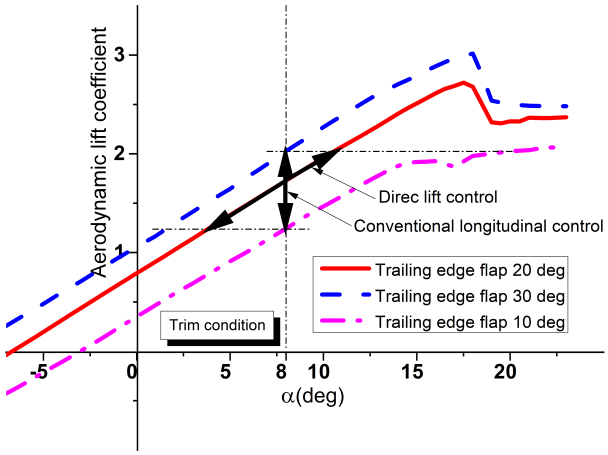

FIGURE 2. Aerodynamic lift changed by direct lift surface or attack of the angle.

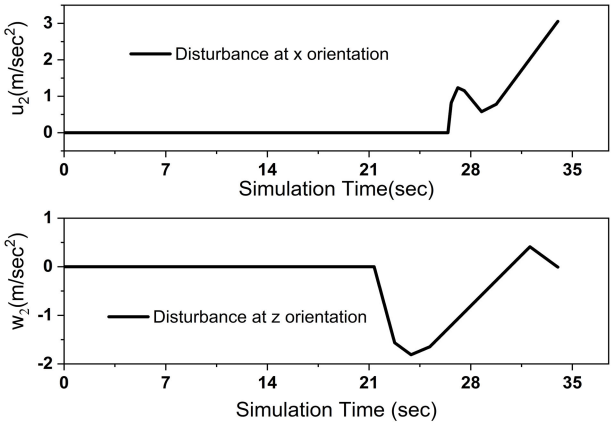

FIGURE 3. The steady coefficients of ship-wake disturbances.

Last but not least, the ship air wake is always the most important disturbance issue in aircraft landing and may introduce more than one arrest rope distance of horizon error (12m). It is important for validating the effectiveness of landing control law [24]. Thus, this paper applies the standard carrier landing disturbance model described in MIL-F-8785C [25]. Although the disturbance simulation model is hard to reflect the reality, the model always is used in analysis and simulation to determine aircraft control response and path control accuracy during carrier aircraft landing. Total disturbance velocities are computed by adding segments caused by random free-air disturbances, u_1, v_1, w_1; steady ship-wake disturbances, u_2, w_2; period ship-motion-induced turbulence, u_3, w_3; and random ship-wake disturbances u_4, v_4, w_4. Fig. 3 displays the most important coefficient of steady ship-wake disturbance, commonly known as ''rooster wake''. The orientation of x and z represent of x and z axis of aircraft body coordinate.

The trajectory dynamic equations can be described as follow, including one order disturbance coefficient.

$$\begin{cases} \dot{V} = (n_x - g_x)\, g + \Delta V_w \\ \dot{\alpha} = -p\cos\alpha\tan\beta + q - r\sin\alpha\tan\beta \\ \quad + \dfrac{g}{V\cos\alpha}\left(n_z + g_z\right) + \Delta\alpha_w \\ \dot{\beta} = p\sin\alpha - r\cos\alpha + \dfrac{g}{V}\left(n_y + g_y\right) + \Delta\beta_w \end{cases} \tag{9}$$

where n_x, n_y and n_z respectively represents the overload coefficients of three axes, which were calculated from the aerodynamic force and engine force in the wind coordination. And g_x, g_y and g_z respectively represents the overload coefficients introduced by gravity and transforms from inertial coordination as follows:

$$\begin{bmatrix} g_x \\ g_y \\ g_z \end{bmatrix} = \boldsymbol{L}_{wb}\boldsymbol{L}_{be}\begin{bmatrix} 0 \\ 0 \\ m \end{bmatrix} \tag{10}$$

where $\boldsymbol{L}_{wb}, \boldsymbol{L}_{be}$ respectively represents the transformation matrix of body frame to wind frame and inertial frame to body frame.

In Eq. (9), the ship air wake disturbances are introduced into the dynamic equations with $\left(\Delta V_w\ \Delta\alpha_w\ \Delta\beta_w\right)$. The one-order dynamics are calculated by the ship air wake speed at three axes of wind coordination.

$$\begin{cases} \Delta V_w = \sqrt{u_{wb}^2 + v_{wb}^2 + w_{wb}^2} \\ \Delta\alpha_w = \dfrac{w_{wb}}{u} \\ \Delta\beta_w = \dfrac{v_{wb}}{V} \end{cases} \tag{11}$$

where $\left(u_{wb}\ v_{wb}\ w_{wb}\right)$ respectively represents air wake disturbance in body coordination. ΔV_w is speed disturbance increment from air wake. $\Delta\alpha_w$ is the attack of angle disturbance increment from air wake and $\Delta\beta_w$ is sideslip angle disturbance increment from air wake.

D. SIGNALS PROCESSING

The sensor measurement module adopts a simple model of zero-order holding and one-step delay to process feedback and measurement information. In the process of incremental dynamic inversion design, the dynamics of the control state measured at the last moment are as follows:

$$\left(\left[\dot{p} \quad \dot{q} \quad \dot{r}\right], \left[\dot{V} \quad \dot{\gamma}\right]\right) \tag{12}$$

The angular rate dynamics and flight speed dynamic are directly used in the simulation dynamic model. $\dot{\gamma}_0$ is obtained through the following steps. Firstly, the glide angle is calculated in the following way:

$$\gamma = -\arcsin\frac{w}{|V_k|} = \arctan\left(\frac{-w}{\sqrt{u^2+v^2}}\right) \tag{13}$$

Derivation Eq. (13):

$$\dot{\gamma} = -\arcsin\frac{w}{|V_k|} = \arctan\left(\frac{-w}{\sqrt{u^2+v^2}}\right)$$

$$= \frac{1}{V_k^2}\left(\frac{w\left(u\dot{u}+v\dot{v}\right)-\dot{w}\left(u^2+v^2\right)}{\sqrt{u^2+v^2}}\right)_e \tag{14}$$

where V_k represents the velocity in the trajectory coordinate frame.

In the case of zero roll angle ($\mu = 0$), the trajectory coordinate coincides with the ground coordinate. At this point, the velocity of $\boldsymbol{V}_e$ is obtained through $\boldsymbol{V}_b$ by the coordinate transformation matrix. At this point, only the velocity derivative in inertial frame is solved by overload as follows:

$$\dot{\boldsymbol{V}}_e = \begin{bmatrix} n_x^e \\ n_y^e \\ n_z^e + 1 \end{bmatrix} g \tag{15}$$

Among Eq. (15), $\left(n_x^e \; n_y^e \; n_z^e\right)$ are the inertial frame triaxial overloads.

Finally, the INDI framework needs to measure the control state dynamic information which can be obtained by current sensor and measurement system.

$$\left(\left[\dot{p} \quad \dot{q} \quad \dot{r}\right], \left[\boldsymbol{V}_e \quad n_x^e \quad n_y^e \quad n_z^e\right]\right) \tag{16}$$

The actuator model of control surfaces used in the landing system is a first-order model with a rate limit:

$$\frac{u_r}{u_c} = \frac{60}{s+60}, \quad u_c^{\max} \le u_c \le u_c^{\min}, \quad -120 \le \dot{u}_c \le 120 \tag{17}$$

where u_c, u_r respectively is control system input instruction and actuator response.

All feedback signals are delayed with one step of simulation time in the landing system.

III. DESIGN OF INDI LANDING CONTROL LAW BASED ON DLC

The mathematical derivation of INDI control law and the INDI+DLC precision landing control architecture will be analyzed in this section. In the first subsection, the comparison between NDI and INDI aircraft control method will be derived in mathematical forms. The second subsection introduces the INDI+DLC precision control design ideal and structures.

A. COMPARISON OF MATHEMATICAL DERIVATION BETWEEN NDI AND INDI

This subsection describes the design procedure of the INDI control law and illustrates that INDI is more robust than NDI in terms of same external disturbance and unmodeled disturbance.

1) INDI CONTROL LAW

Assuming that general nonlinear system can be written as affine nonlinear system:

$$\begin{aligned} \dot{\boldsymbol{x}} &= \boldsymbol{f}(\boldsymbol{x}) + \boldsymbol{G}(\boldsymbol{x})\boldsymbol{u} \\ \boldsymbol{y} &= \boldsymbol{h}(\boldsymbol{x}) \end{aligned} \tag{18}$$

where $\boldsymbol{f} \in \boldsymbol{R}^{n\times n}$, $\boldsymbol{h} \in \boldsymbol{R}^{n\times p}$, $\boldsymbol{G} \in \boldsymbol{R}^{n\times m}$.

The output dynamic equation of affine nonlinear systems is written as follow [28]:

$$\boldsymbol{y}^{(\rho)} = \boldsymbol{\alpha}(\boldsymbol{x}) + \boldsymbol{\mathcal{B}}(\boldsymbol{x})\boldsymbol{u} \tag{19}$$

Expanding the output dynamic at $t - \Delta t$ (subscript 0), the ρ order derivative is:

$$\begin{aligned} \boldsymbol{y}^{(\rho)} &= \boldsymbol{\alpha}(\boldsymbol{x}) + \boldsymbol{\mathcal{B}}(\boldsymbol{x})\boldsymbol{u} \\ &= \boldsymbol{y}_0^{(\rho)} + \left.\frac{\partial\left[\boldsymbol{\alpha}(\boldsymbol{x}) + \boldsymbol{\mathcal{B}}(\boldsymbol{x})\boldsymbol{u}\right]}{\partial \boldsymbol{x}}\right|_0 \Delta\boldsymbol{x} + \boldsymbol{\mathcal{B}}(\boldsymbol{x}_0)\boldsymbol{u} + \boldsymbol{O}\left(\Delta\boldsymbol{x}^2\right) \\ &= \boldsymbol{y}_0^{(\rho)} + \boldsymbol{\mathcal{B}}(\boldsymbol{x}_0)\Delta\boldsymbol{u} + \delta(z, \Delta t) \end{aligned} \tag{20}$$

where $\Delta\boldsymbol{u}$, $\Delta\boldsymbol{x}$ respectively represents control and state increment within a time step Δt.

$$\delta(z, \Delta t) = \left[\left.\frac{\partial\left[\boldsymbol{\alpha}(\boldsymbol{x}) + \boldsymbol{\mathcal{B}}(\boldsymbol{x})\boldsymbol{u}\right]}{\partial \boldsymbol{x}}\right|_0 \Delta\boldsymbol{x} + \boldsymbol{O}\left(\Delta\boldsymbol{x}^2\right)\right]_{x=T^{-1}(z)} \tag{21}$$

At this point the control increment is:

$$\Delta\boldsymbol{u} = \boldsymbol{\mathcal{B}}^{-1}(\boldsymbol{x}_0)\left(\boldsymbol{v} - \boldsymbol{y}_0^{(\rho)}\right) \tag{22}$$

Because the characteristics of aircraft nonlinear dynamic equations, the relation order ρ is 1. And $\boldsymbol{y}_0$ general represents the desired dynamic of control state and obtained by the means of measurement system.

The total control surface input is:

$$\boldsymbol{u} = \boldsymbol{u}_0 + \Delta\boldsymbol{u} \tag{23}$$

the control input vector $\boldsymbol{u}_0$ is from last step. By substituting the above formula into Eq. 16, the following relation is obtained:

$$\boldsymbol{y}^{(\rho)} = \boldsymbol{v} + \delta(z, \Delta t) \tag{24}$$

From Eq.24, if the dynamic equation of the output control state ignores the higher-order term, the controlled-state's dynamic equation simplified as a pure integral pseudo-linear system by the inversion feedback method.

By using the homeomorphism mapping, the closed-loop system used by the incremental dynamic inversion method is obtained as follow [28]:

$$\begin{aligned} \dot{\boldsymbol{\eta}} &= \boldsymbol{f}_0(\boldsymbol{\eta}, \boldsymbol{\xi}) \\ \dot{\boldsymbol{\xi}} &= \boldsymbol{A}_c\boldsymbol{\xi} + \boldsymbol{B}_c\left[\boldsymbol{v} + \delta(z, \Delta t)\right] \\ \boldsymbol{y} &= \boldsymbol{C}_c\boldsymbol{\xi} \end{aligned} \tag{25}$$

The rigorous mathematical expressions of NDI and INDI in the output state channel can be obtained by the homeomorphic mapping method that the nonlinear state dynamic equations can be transformed into an independent expression with external and internal state, respectively. From the closed-loop system of Eq. (25), it is obvious that the dynamic equations of the internal states still contain the external states' quantity. While for the controlled external states, it is independent. Generally, NDI mainly relies on the accurate model dynamic feedback to eliminate the actual coupling relation of control states. In contrast, Eq. (25) indicate that INDI mainly

feedbacks control state and the position of the control input measured at the last moment to realize the closed-loop incremental control, no need to feedback the dynamic information of aircraft state.

2) ANALYSIS OF INDI ROBUSTNESS

This subsection briefly illustrate that the INDI control framework is more robust than the NDI control framework. Firstly, the full-state nonlinear system of aircraft is subjected to external disturbances, as below show:

$$\begin{aligned} \dot{\boldsymbol{x}} &= \boldsymbol{f}(\boldsymbol{x}) + \boldsymbol{G}(\boldsymbol{x})\boldsymbol{u} + \boldsymbol{d} \\ \boldsymbol{y} &= \boldsymbol{H}(\boldsymbol{x} - \boldsymbol{x}_*) \end{aligned} \tag{26}$$

the Boolean selection matrix $\boldsymbol{H}$ mostly is unit diagonal matrix. Defining $\boldsymbol{x}_*$ is $\boldsymbol{x}$ neighborhood state point. According to Eq. (25), $\xi = [p; q; r]$, $\xi_i = h_i(x) = x_i - x_{i*}$. At this point, the relative order of each output channel is $\rho_i = 1$, because the relative order of each output channel is 1st, the three-axis angular rate states of aircraft are selected as the external control states, specifically, the dynamic state of external state is:

$$\dot{\boldsymbol{y}} = \dot{\boldsymbol{\xi}} = \bar{\boldsymbol{f}}(\boldsymbol{\xi}) + \bar{\boldsymbol{G}}(\boldsymbol{\xi})\boldsymbol{u} + \boldsymbol{H}\boldsymbol{d} \tag{27}$$

The external state vector is then expanded as first-order Taylor series at the previous moment:

$$\begin{aligned} \dot{\boldsymbol{\xi}} &= \bar{\boldsymbol{f}}(\boldsymbol{\xi}) + \bar{\boldsymbol{G}}(\boldsymbol{\xi})\boldsymbol{u} + \boldsymbol{H}\boldsymbol{d} \\ &= \dot{\boldsymbol{\xi}}_0 + \left.\frac{\partial\left[\bar{\boldsymbol{f}}(\boldsymbol{\xi}) + \bar{\boldsymbol{G}}(\boldsymbol{\xi})\boldsymbol{u}\right]}{\partial\boldsymbol{\xi}}\right|_0 \Delta\boldsymbol{\xi} + \bar{\boldsymbol{G}}\left(\boldsymbol{\xi}_0\right)\Delta\boldsymbol{u} \\ &\quad + \boldsymbol{H}\Delta\boldsymbol{d} + O\left(\Delta\boldsymbol{\xi}^2\right) \\ &= \dot{\boldsymbol{\xi}}_0 + \bar{\boldsymbol{G}}\left(\boldsymbol{\xi}_0\right)\Delta\boldsymbol{u} + \boldsymbol{H}\Delta\boldsymbol{d} + \delta(\boldsymbol{\xi}, \Delta t) \end{aligned} \tag{28}$$

At this point, when $\exists t_1, \forall \Delta t \leq t_1$, the partial derivative of the second order is ignored, the incremental nonlinear dynamic inversion control law is:

$$\Delta\boldsymbol{\mu} = \bar{\boldsymbol{G}}^{-1}\left(\boldsymbol{\xi}_0\right)\left(\boldsymbol{v} - \boldsymbol{\xi}_0\right) \tag{29}$$

The dynamic equations of the external and internal states of the closed-loop system are:

$$\begin{aligned} \dot{\boldsymbol{\xi}} &= \boldsymbol{v} + \boldsymbol{H}\Delta\boldsymbol{d} + \delta(\boldsymbol{\xi}, \Delta t) \\ \dot{\boldsymbol{\eta}} &= \frac{\partial\boldsymbol{\Phi}}{\partial\boldsymbol{x}}\left(\boldsymbol{f}(\boldsymbol{x}) + \boldsymbol{G}(\boldsymbol{x})\boldsymbol{u} + \boldsymbol{d}\right) = \frac{\partial\boldsymbol{\Phi}}{\partial\boldsymbol{x}}\left(\boldsymbol{f}(\boldsymbol{x}) + \boldsymbol{d}\right) = \boldsymbol{f}_d(\boldsymbol{\eta}, \boldsymbol{\xi}, \boldsymbol{d}) \end{aligned} \tag{30}$$

From Eq. (30), the effect of disturbance on the external states is through increment $\Delta\boldsymbol{d}$, while, directly to the internal states with absolute value $\boldsymbol{d}$. Generally speaking, assuming the disturbance quantity is continuous when the increment step Δt is very small, there is $\lim_{\Delta t \to 0} \|\boldsymbol{d}\|_2 = 0$, and if $\boldsymbol{d} \neq 0, \exists \Delta t, \|\Delta\boldsymbol{d}\|_2 < \|\boldsymbol{d}\|_2$, we can see that through the increment control, the disturbance term of the system is compensated by the measurement system at each update time so that the original larger disturbance term becomes smaller increment disturbances.

Assuming that there is unmodeled error in the system itself, the NDI control law input is as follow:

$$\begin{aligned} \boldsymbol{u} &= \dot{\boldsymbol{\xi}} = \bar{\boldsymbol{f}}(\boldsymbol{\xi}) \\ &\quad + \Delta\bar{\boldsymbol{f}}(\boldsymbol{\xi}) + \left[\bar{\boldsymbol{G}}(\boldsymbol{\xi}) + \Delta\bar{\boldsymbol{G}}(\boldsymbol{\xi})\right]\left[\bar{\boldsymbol{G}}(\boldsymbol{\xi})^{-1}\left(\dot{\boldsymbol{\xi}}_d - \bar{\boldsymbol{f}}(\boldsymbol{\xi})\right)\right] \\ &= \dot{\boldsymbol{\xi}}_d + \left(\Delta\bar{\boldsymbol{f}} + \Delta\bar{\boldsymbol{G}}\bar{\boldsymbol{G}}^{-1}\dot{\boldsymbol{x}}_d - \Delta\bar{\boldsymbol{G}}\bar{\boldsymbol{G}}^{-1}\bar{\boldsymbol{f}}(x)\right)_{\text{mismatch}} \end{aligned} \tag{31}$$

the vector $\Delta\bar{\boldsymbol{f}}(\boldsymbol{\xi})$ is the inversion feedback system error. The inversion feedback system error highly depends on the system model and leads to the instability of the closed system.

The input of the INDI control law is:

$$\begin{aligned} \boldsymbol{u} &= \dot{\boldsymbol{\xi}} = \dot{\boldsymbol{\xi}}_0 + \left[\bar{\boldsymbol{G}}(\boldsymbol{\xi}) + \Delta\bar{\boldsymbol{G}}(\boldsymbol{\xi})\right]\left[\bar{\boldsymbol{G}}(\boldsymbol{\xi})^{-1}\left(\dot{\boldsymbol{\xi}}_d - \dot{\boldsymbol{\xi}}_0\right)\right] \\ &= \dot{\boldsymbol{\xi}}_d + \left(\Delta\bar{\boldsymbol{G}}\bar{\boldsymbol{G}}^{-1}\dot{\boldsymbol{\xi}}_d - \Delta\bar{\boldsymbol{G}}\bar{\boldsymbol{G}}^{-1}\dot{\boldsymbol{\xi}}_0\right)_{\text{mismatch}} \end{aligned} \tag{32}$$

As discussed above, NDI is employed to eliminate the nonlinear characteristics of aircraft by inversion feedback. Thus, the limitation is that the obtained closed-loop control system requires the pre-knowledge of model dynamics. Consequently, it highly depends on the model and has poor robustness. However, INDI directly forms a closed-loop system through incremental inversion feedback, the requirements mainly is reflected in the measurement and feedback system. The higher requirements on the measurements of controlled state dynamics contribute to the lower dependence on the information of the aircraft model. Thus, the robustness is higher.

B. INDI + DLC CONTROL LAW DESIGN

This subsection introduces the design of landing control law with DLC based on the incremental dynamic inversion framework for carrier aircraft. Firstly, according to the 6-DOF dynamic equations of the aircraft, the incremental dynamic inversion control law is designed in the trajectory loop and attitude loop, respectively, and then, two-layer parallel inversion feedback loops are formed, as demonstrated in Fig. 4.

The dynamic inversion controller mainly selects NDI and INDI. It is clear that the NDI controller relies more on the aerodynamic model, need to eliminate the dynamics of the aircraft control states, and thus can input the desired dynamics through the reference model of the command loop and trajectory loop to achieve the purpose of controlling the state transition characteristic (see Fig. 4). The INDI control loop mainly relies on the dynamics of the last-moment control state estimated by the measurement system and continuously corrects the error to realize the incremental control (see Fig. 4). Based on the design of the two-layer parallel dynamic inversion loops, this paper designs two matching control allocation modules to isolate the direct lift surface and thrust actuator from the conventional control surfaces (elevators, ailerons, rudders) in different control allocation loops. At the same time, the design is compatible with the introduction of more redundant control surfaces in the future.

Fig. 5 illustrates the INDI control framework. The control increments are solved by the compensation reference loop

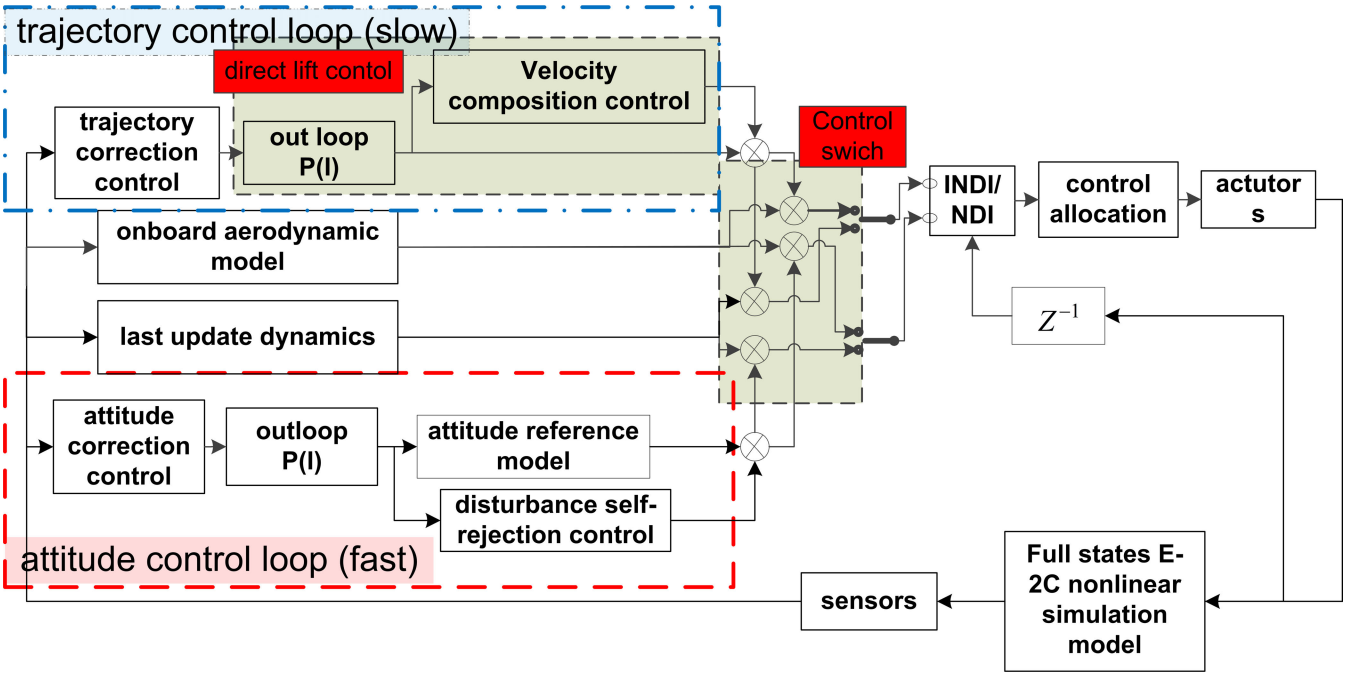

FIGURE 4. The block diagram of the landing control law with the direct lift control based on the incremental dynamic inversion framework.

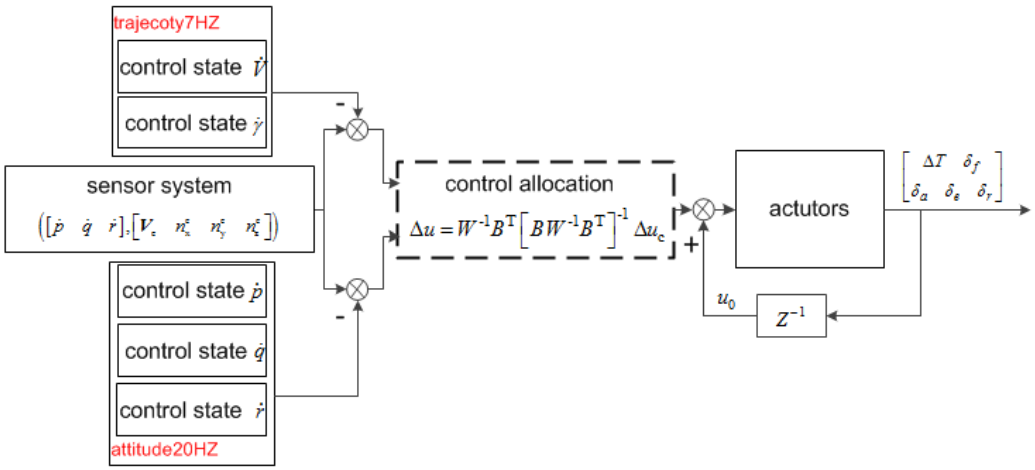

FIGURE 5. The control block diagram of the incremental dynamic inversion control loop.

and commander loop, and then the incremental dynamic inversion control inputs are computed by directly adding the zero-hold actuator value at the last moment with the one-step delay. The compensation loop, including the reference model, is respectively designed for each controlled channel in the flight path (trajectory) loop and attitude loop, as demonstrated in Figs. 6 and 7.

In order to increase the anti-disturbance ability of inversion feedback loop, the anti-disturbance loop is added in the attitude loop. In order to stabilize landing velocity, the throttle compensation module is added in the flight path control loop to ensure a specific sinking rate in the phase of carrier aircraft landing.

As for the onboard aerodynamic computation (OBAC) model depicted in Fig. 4, we use a linear model as OBAC because most attitude states are stable at the landing phase. Moreover, the main reason is that the control envelope is so small at the landing mode. The linear model of OBAC is coming from the aircraft system dynamics matrix and control effectiveness matrix extracted by using small disturbance theory. The aircraft system dynamic matrix $(\boldsymbol{A}_{\text{attitude}}, \boldsymbol{A}_{\text{trajectory}})$ and control effectiveness matrix $(\boldsymbol{B}_{\text{attitude}}, \boldsymbol{B}_{\text{trajectory}})$ are given as: $(\boldsymbol{A}_{\text{attitude}})$, shown at the bottom of the next page.

IV. IMPLEMENTATION OF INDI + DLC CONTROL LAW

In this section, the implementation of INDI+DLC control law will be described as designed sequence. Firstly, "time scale separation" principle of INDI+DLC will be introduced, and then, attitude stabilization control law and direct lift control law will be designed separately. For the completement of

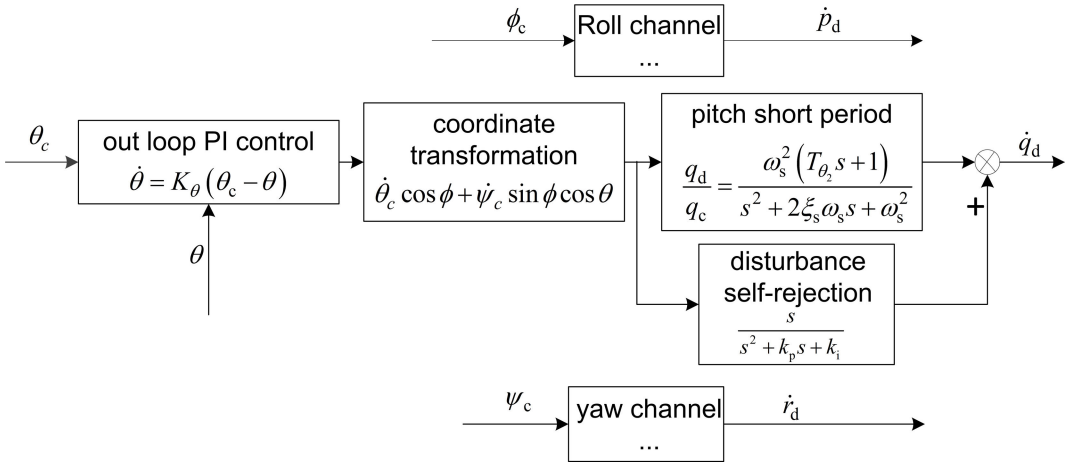

FIGURE 6. The block diagram of incremental dynamic inversion attitude compensation reference loop.

INDI+DLC, the internal loop anti-disturbance control loop, internal loop reference model and external instruction loop will be also designed.

A. "TIME SCALE SEPARATION" PRINCIPLE OF INDI + DLC

The mathematical expression of the dynamic ignore terms of dynamic inversion is obtained by the nonlinear homeomorphism mapping as previous section mentioned. The stability and robustness of the inversion feedback controller are closely related to the neglect terms [26], [27]. However, the inversion feedback control is still designed based on the "time scale separation" principle. In this way, the dynamic inversion control method is easy to understand for engineers, and the dynamic equations can be simplified into two sets of equations according to the long-and-short period characteristic of aircraft equation itself, i.e., the force equation and the moment equation. Then according to the integral state relationship, the attitude and trajectory control states are isolated in different frequency bandwidths according to different update frequencies. It is considered that the values of the trajectory state are steady when the values of the attitude state are updating, and the values of the trajectory state can be corrected quickly by the attitude states. Consequently, the control states are divided into "fast and slow" dynamics according to different update frequency bandwidths, as Fig. 8 shows.

B. ATTITUDE STABILIZATION LOOP

This section gives the implementation of the NDI/INDI control law in the attitude stabilizing loop demonstrated in Fig 6. Firstly, the aircraft attitude equation is expanded according to the output [29]:

$$\dot{\boldsymbol{y}} = \frac{\partial \boldsymbol{h}(\boldsymbol{x},\boldsymbol{p})}{\partial \boldsymbol{x}} \frac{d\boldsymbol{x}}{dt} = L_f \boldsymbol{h}(\boldsymbol{x},\boldsymbol{p}) + L_G \boldsymbol{h}(\boldsymbol{x},\boldsymbol{p})\boldsymbol{u} \tag{33}$$

The corresponding control law is:

$$\boldsymbol{u} = L_G \boldsymbol{h}(\boldsymbol{x},\boldsymbol{p})^{-1}\left(v - L_f \boldsymbol{h}(\boldsymbol{x},\boldsymbol{p})\right) \tag{34}$$

The attitude dynamic equation of Eq. (1) can be written directly as affine nonlinear form:

$$\dot{\boldsymbol{\omega}} = \underbrace{-\boldsymbol{J}(\boldsymbol{p})^{-1}\boldsymbol{\omega} \times \boldsymbol{J}(\boldsymbol{p})\boldsymbol{\omega}}_{f_M(\boldsymbol{x},\boldsymbol{p})} + \underbrace{\boldsymbol{J}(\boldsymbol{p})^{-1}\left(\boldsymbol{M}_{\mathrm{A}}(\boldsymbol{x},\boldsymbol{u},\boldsymbol{p}) + \boldsymbol{M}_{\mathrm{T}}(\boldsymbol{x},\boldsymbol{u})\right)}_{G_M(\boldsymbol{x},\boldsymbol{p})\boldsymbol{u}} \tag{35}$$

After linearizing the above equations, the three-axis angular rate dynamic model can be rewritten as follow:

$$\dot{\boldsymbol{x}}_m = \boldsymbol{f}_M(\boldsymbol{x}_{\mathrm{m}},\boldsymbol{p}) + \boldsymbol{G}_M(\boldsymbol{x}_m,\boldsymbol{p})\boldsymbol{u} \tag{36}$$

$$\boldsymbol{A}_{\text{attitude}} = \begin{bmatrix} 0.00 & 0.14 & 0.00 & -1.76 & 0.00 & 1.74 & -0.13 & 0.00 & 0.93 & 0.00 & 0.00 & 0.00 & 0.00 & -0.93 \\ -0.27 & 0.11 & 0.00 & 0.00 & -0.98 & 0.00 & -0.06 & -0.34 & 0.40 & 0.00 & 0.00 & 0.00 & 0.34 & -0.40 \\ -0.13 & -0.04 & 0.00 & -0.22 & 0.00 & -0.13 & 0.04 & 0.00 & -0.31 & 0.00 & 0.00 & 0.00 & 0.00 & 0.31 \end{bmatrix}$$

$$\boldsymbol{A}_{\text{trajectory}} = \begin{bmatrix} -0.05 & -0.10 & 0.00 & 0.00 & 0.00 & 0.00 & 0.00 & 0.00 & 0.00 & 0.00 & 0.00 & 0.00 & -0.17 & 0.00 \\ 0.34 & 1.95 & 0.00 & 0.00 & 0.00 & 0.00 & 0.00 & -1.25 & -0.01 & 0.00 & 0.00 & 0.00 & 1.25 & 0.01 \end{bmatrix}$$

$$\boldsymbol{B}_{\text{attitude}} = \begin{bmatrix} -0.01 & -4.44 & 0.11 \\ -2.27 & 0.12 & 0.19 \\ 0.03 & -0.19 & -1.59 \end{bmatrix}$$

$$\boldsymbol{B}_{\text{trajectory}} = \begin{bmatrix} -0.04 & 0.06 \\ 0.21 & 0.06 \end{bmatrix}$$

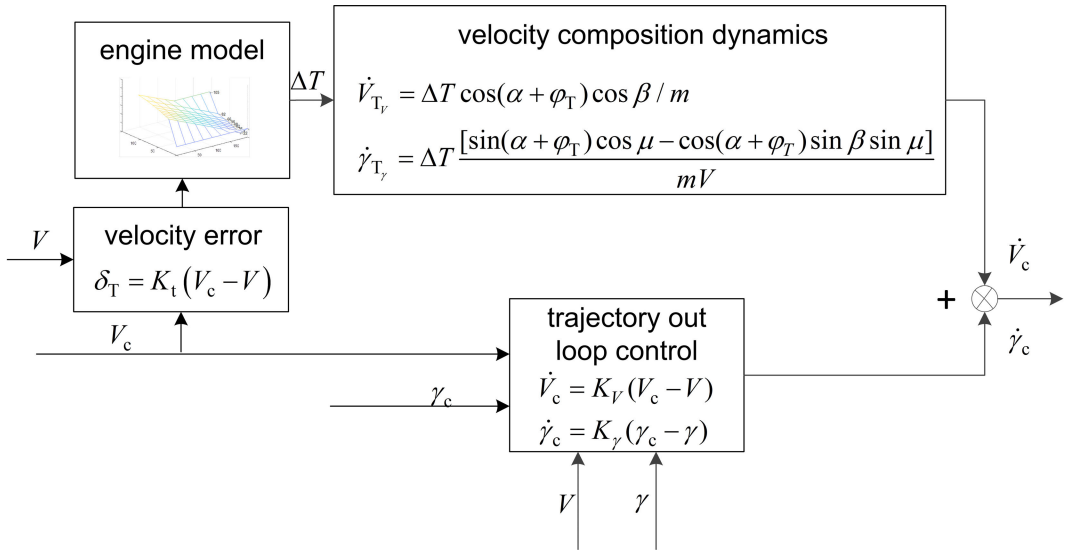

FIGURE 7. The block diagram of incremental dynamic inversion trajectory compensation reference loop.

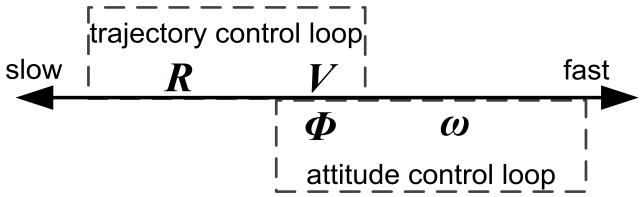

FIGURE 8. The comparison graph of controlled states updating speed.

where $\boldsymbol{x}_{\mathrm{m}} \in \boldsymbol{R}^n$ is the control state vector, $\boldsymbol{u} \in \boldsymbol{R}^m$ is the control vector, $\boldsymbol{y}_{\mathrm{m}} \in \boldsymbol{R}^n$ is the control output vector and $\boldsymbol{f}_M \in \boldsymbol{R}^{n\times n}$ is the system matrix, $\boldsymbol{G}_M \in \boldsymbol{R}^{n\times m}$ is the control effectiveness matrix. When the control vector dimension exceeds the control output variables, $m > n$, a control allocation algorithm always is needed to deal with the problem of redundant control surfaces.

Thus, the control law of NDI is rewritten as:

$$\boldsymbol{u}_{\mathrm{m}}^{\mathrm{NDI}}(t) = G_{\mathrm{M}}^{-1}\left(\dot{\boldsymbol{x}}_{\mathrm{m}}^{\mathrm{des}} - \boldsymbol{f}_{\mathrm{M}}\left(\boldsymbol{x}_{\mathrm{m}}\left(t\right)\right)\right) \tag{37}$$

The INDI control law is obtained by writing the aircraft attitude equation into an incremental form. Firstly, the first-order Taylor expansion of the aircraft equation is expended at the last moment $t_0 = t - \Delta t$ (represented by the superscript "0"):

$$\begin{aligned}\dot{\boldsymbol{x}}_{\mathrm{m}} = \dot{\boldsymbol{x}}_{\mathrm{m}}^0 &+ \frac{\partial}{\partial \boldsymbol{x}}\left[\boldsymbol{f}_M(\boldsymbol{x}_{\mathrm{m}},\boldsymbol{p})\right. \\ &\left.+\boldsymbol{G}_M(\boldsymbol{x}_{\mathrm{m}},\boldsymbol{p})\boldsymbol{u}\right]\big|_{\boldsymbol{x}=\boldsymbol{x}^0,\boldsymbol{u}=\boldsymbol{u}^0}\underbrace{\left(\boldsymbol{x}_{\mathrm{m}}-\boldsymbol{x}_{\mathrm{m}}^0\right)}_{\Delta\boldsymbol{x}_{\mathrm{m}}} \\ &+\frac{\partial}{\partial \boldsymbol{u}}\left[\boldsymbol{f}_M(\boldsymbol{x}_{\mathrm{m}},\boldsymbol{p})+\boldsymbol{G}_M(\boldsymbol{x}_{\mathrm{m}},\boldsymbol{p})\boldsymbol{u}\right]\big|_{\boldsymbol{x}=\boldsymbol{x}^0,\boldsymbol{u}=\boldsymbol{u}^0}\underbrace{\left(\boldsymbol{u}-\boldsymbol{u}^0\right)}_{\Delta\boldsymbol{u}}\end{aligned} \tag{38}$$

In practical, the "time-scale separation" is guaranteed. At this point, the change of states is very small relative to the control, and satisfied as follow:

$$\boldsymbol{x}_{\mathrm{m}} - \boldsymbol{x}_{\mathrm{m}}^0 \ll \boldsymbol{u} - \boldsymbol{u}^0 \tag{39}$$

Thus, the dynamic equation of angular rate loop is simplified as follow:

$$\dot{\boldsymbol{x}}_{\mathrm{m}} = \dot{\boldsymbol{x}}_{\mathrm{m}}^0 + \boldsymbol{G}_M(\boldsymbol{x}_{\mathrm{m}}^0,\boldsymbol{p})\Delta\boldsymbol{u} \tag{40}$$

According to the above expression, the output vector of reference model $\dot{\boldsymbol{x}}_m$ will be replaced by $\dot{\boldsymbol{x}}_m^{des}$, and the control law of INDI will be solved as follow:

$$\boldsymbol{u}_{\mathrm{m}}^{\mathrm{INDI}}(t) = \boldsymbol{u}_{\mathrm{m}}^0 + \boldsymbol{G}_{\mathrm{M}}(\boldsymbol{x}_{\mathrm{m}}^0,\boldsymbol{p})^{-1}\left(\dot{\boldsymbol{x}}_{\mathrm{m}}^{\mathrm{des}} - \dot{\boldsymbol{x}}_{\mathrm{m}}^0\right) \tag{41}$$

And then, the Eq. (41) can be expressed in the following form:

$$\boldsymbol{u}_{\mathrm{m}}^{\mathrm{INDI}}(t) = \delta_{\mathrm{m}}^0 + \underbrace{M_{c\delta}\left(x,p\right)J(p)}_{\boldsymbol{G}_M(\omega_{\mathrm{m}}^0,\hat{\boldsymbol{p}})^{-1}}\left(\dot{\omega}_{\mathrm{m}}^{\mathrm{des}} - \frac{\dot{\omega}_{\mathrm{m}}^0}{\hat{x}_{\mathrm{m}}^0}\right) \tag{42}$$

where $M_{c\delta}$ is the effectiveness matrix of conventional control surfaces (aileron, rudder, elevator).

C. DIRECT LIFT CONTROL LOOP

This subsection gives the implementation of the NDI/INDI control law in the trajectory tracking loop demonstrated in Fig 7. General aerodynamic calculation contains the attack angle α and β, therefore, the dynamic equations represented by the state $\boldsymbol{V}$ of the aircraft system are transformed into the form expressed with $\left[\begin{array}{ccc} V & \alpha & \beta \end{array}\right]^T$ in the wind coordinate. Moreover, the design goal of this paper is the precision trajectory control of the carrier landing based on the direct lift, so the dynamic relationship of the force equation is expressed by the state of the flight path angle $\left[\begin{array}{ccc} V & \gamma & \chi \end{array}\right]^T$. In other hand,

the control states of the carrier aircraft glide-landing mission are the track glide angle γ and the landing speed V, which can ensure the desired glide path and stable landing speed of carrier aircraft. While, the trajectory azimuth angle χ is not discussed for the internal dynamics of the aircraft. At this point, the trajectory (flight path) equations of Eq. (1) are expressed in the trajectory coordinate as follow:

$$\begin{aligned}\dot{V} &= -g\sin\gamma \\ &\quad + \frac{1}{m}\left[\left(C_{T_{\Delta s}}\Delta s + T_0\right)\cos(\alpha+\varphi_T)\cos\beta - D\left(\Delta s, \delta f\right)\right] \\ \dot{\gamma} &= \frac{-g\cos\gamma}{V} \\ &\quad - \frac{1}{mV}\left[Y\left(\Delta s, \delta f\right)\sin\mu + \left(C_{L_{\delta f}}\delta f + L_0\right)\cos\mu\right] \\ &\quad + \frac{1}{mV}\left[\left(C_{T_{\Delta s}}\Delta s + T_0\right)\left[\sin(\alpha+\varphi_T)\cos\mu\right.\right. \\ &\quad \left.\left. - \cos(\alpha+\varphi_T)\sin\beta\sin\mu\right]\right] \end{aligned} \tag{43}$$

where δf is direct lift surface deflection, $C_{L_{\delta f}}$ is lift coefficient produced by direct lift surface deflection, Δs is throttle opening deflection, $C_{T_{\Delta s}}$ is thrust coefficient by throttle opening. Obviously, the equations of state cannot be written directly as affine nonlinear system and expressed as general nonlinear system [30]:

$$\dot{\boldsymbol{x}}_{\mathrm{f}} = f\left(\boldsymbol{x}, \boldsymbol{x}_{\mathrm{f}}, \boldsymbol{u}_{\mathrm{f}}\right) \tag{44}$$

where $\boldsymbol{x}_{\mathrm{f}} = [V \quad \gamma]^{\mathrm{T}}$, $\boldsymbol{u}_{\mathrm{f}} = [\delta f \quad \Delta s]^{\mathrm{T}}$.

In order to realize the basic form of inversion system, the above nonlinear equations are linearized according to the small perturbation principle in the position of landing attitude $\boldsymbol{x}_*$ and trim position of landing speed $\boldsymbol{u}_*$. The NDI control laws are designed by using the linearized equations, and the state space equation is obtained:

$$\dot{\boldsymbol{x}}_{\mathrm{f}} = \boldsymbol{A}_{\mathrm{F}}\boldsymbol{x}_{\mathrm{f}} + \boldsymbol{B}_{\mathrm{F}}u_{\mathrm{f}} \tag{45}$$

where $\boldsymbol{A}_F$ is system matrix, $\boldsymbol{B}_F$ is the control effectiveness matrix. At this point, the NDI control law is:

$$\boldsymbol{u}_{\mathrm{m}}^{\mathrm{NDI}}(t) = \boldsymbol{B}_{\mathrm{F}}^{-1}\left(\dot{\boldsymbol{x}}_{\mathrm{m}}^{\mathrm{des}} - \boldsymbol{A}_{\mathrm{F}}\boldsymbol{x}_{\mathrm{f}}\right) \tag{46}$$

Additionally, the linear equation of state obtained under the condition of landing is written as an incremental form:

$$\dot{\boldsymbol{x}}_{\mathrm{f}} = \dot{\boldsymbol{x}}_{\mathrm{f}}^0 + \boldsymbol{A}_{\mathrm{F}}\underbrace{\left(\boldsymbol{x}_{\mathrm{f}} - \boldsymbol{x}_{\mathrm{f}}^0\right)}_{\Delta\boldsymbol{x}_{\mathrm{m}}} + \boldsymbol{B}_{\mathrm{F}}\underbrace{\left(u_{\mathrm{f}} - u_{\mathrm{f}}^0\right)}_{\Delta\boldsymbol{u}} \tag{47}$$

The corresponding INDI control law is obtained as follow:

$$\boldsymbol{u}_{\mathrm{f}}^{\mathrm{INDI}}(t) = \boldsymbol{u}_{\mathrm{f}}^0 + \boldsymbol{B}_{\mathrm{F}}^{-1}\left(\dot{\boldsymbol{x}}_{\mathrm{f}}^{\mathrm{des}} - \dot{\boldsymbol{x}}_{\mathrm{f}}^0\right) \tag{48}$$

D. INTERNAL LOOP ANTI-DISTURBANCE DESIGN

As showed in Fig. 4, the reference model that reflects the short-period characteristics of the aircraft is added to the internal angular rate loop. When using (I)NDI, the nonlinear equation of the aircraft is derived with nonlinear theory. The external control state ($\boldsymbol{\xi}$) is decoupled from the internal state ($\boldsymbol{\eta}$), as shown in Eq. (25). But before mapping, even if $\boldsymbol{\xi} = \begin{bmatrix} p & q & r \end{bmatrix}^T$, the dynamic equations of internal and external states contain coupling terms. Therefore, an anti-disturbance module needs to be added at each angular rate channel, as shown in Fig. 9.

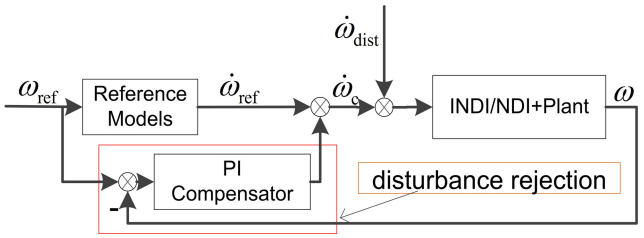

FIGURE 9. The block diagram of disturbance rejection at internal angular rate loop.

Assuming that the dynamics of the real aircraft cannot be completely eliminated with modeled aircraft information, there is a disturbance d. It is corrected by PI compensation, as shown below:

$$\left[-\left(k_{\mathrm{p}} + \frac{k_{\mathrm{i}}}{s}\right)\omega + d\right]\frac{1}{s} = \omega \tag{49}$$

The transfer function of the disturbances is obtained:

$$\frac{\omega}{d} = \frac{1}{s + \left(k_{\mathrm{p}} + k_{\mathrm{i}}/s\right)} = \frac{s}{s^2 + k_{\mathrm{p}}s + k_{\mathrm{i}}} \tag{50}$$

where k_p and k_i are adjustable gain coefficients. It is important to note that the cut-off frequency of the anti-interference module should be consistent with the reference model to ensure that the two modules are compatible. Therefore, the corresponding coefficients should be adjusted to ensure that they are consistent with the zero poles of the reference model described in the subsection E:

$$\begin{aligned} K_{\mathrm{i}} &= 2\zeta\omega_{\mathrm{s}} \\ K_{\mathrm{p}} &= \omega_{\mathrm{s}}^2 \end{aligned} \tag{51}$$

It is necessary to note that the reference model of some channels is first-order, $k_{\mathrm{i}} = 0$. Thus, the corresponding disturbance suppression module must be first-order.

E. INTERNAL LOOP REFERENCE MODEL

As demonstrated in Fig. 4, the reference models that reflect the short-period characteristics of the aircraft are added to the internal angular rate loops. In the pitch angle rate loop, a reference model that accords with the aircraft's characteristics is introduced. In this way, the decoupled system is more in line with the pilot's control experience. The inherent characteristics of the aircraft are added into the closed-loop control loop after decoupling. And the short-period equivalent model, which mainly embodies the motion characteristics of the aircraft's angular rate, is added into the control loop, which suppresses the long-period characteristics and makes the whole control channel cleaner. Finally, the control design quite meets the requirements of precision carrier landing.

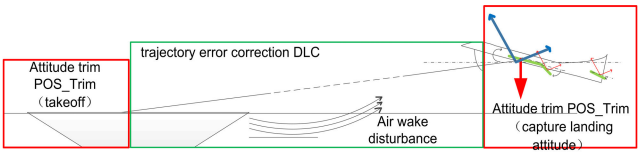

FIGURE 10. The logical functions of two command design.

In the loop of pitch, a second-order equivalent model of the shot period is generally adopted.

$$\frac{q_{\mathrm{d}}}{q_{\mathrm{c}}} = \frac{\omega_{\mathrm{s}}^2\left(T_{\theta_2}s+1\right)}{s^2+2\xi_{\mathrm{s}}\omega_{\mathrm{s}}s+\omega_{\mathrm{s}}^2} \tag{52}$$

when T_{θ_2} is zero, the zero point is removed from the transfer function.

The roll channel is added with a first-order reference model that reflects the short period of roll in the internal angular rate loop. While the Dutch roll and Spiral mode characteristics are ignored. The reference model of roll channel is designed in stability coordinate frame so that the angle of attack of the aircraft will not be transformed into a side slip angle when the nose of the aircraft is rotated. The reference model is as follow:

$$\frac{p_{\mathrm{s,d}}}{p_{\mathrm{s,c}}} = \frac{\omega_{\mathrm{p}}}{s+\omega_{\mathrm{p}}} \tag{53}$$

The directional control uses lateral overload caused by the pedal action to realize the coordinated turn. Thus, the sideslip angle $\dot{\beta} \approx 0$. The first-order dynamic model is used to generate the dynamics of the loop in the yaw angle rate.

$$\frac{r_{\mathrm{s,d}}}{r_{\mathrm{s,c}}} = \frac{\omega_{\mathrm{r}}}{s+\omega_{\mathrm{r}}} \tag{54}$$

The expected yaw angle rate commander $r_{\mathrm{s,c}}$ is designed according to the yaw angle dynamic of the aircraft in stability coordinate frame.

F. EXTERNAL LOOP AND INSTRUCTION LOOP

At last, the essential part of landing control system described in Fig. 4 is the command loop. To demonstrate the ability to quickly correct trajectory errors and decouple controlled states with the direct lift, the function design of the command loop is of great significance to the exploitation of full potential of this paper designed control framework [3]. In this paper, two parts are designed in the command loop, i.e., the direct lift module (DLC) and landing attitude adjustment module (POS_Trim), according to the process the characteristic of the control system at landing stage. The POS_Trim command loop is used for attitude stabilization when establishing landing attitude at entering landing windows or taking off with landing failure. The DLC module enables the aircraft to capture and correct the flight path error in the expected landing attitude. This significantly simplifying landing operation tasks. The logical functions of the command loop in the landing mission are indicated in Fig. 10.

The functions of two command control loops respectively are that the POS_Trim control loop is to realize the attitude

FIGURE 11. Simulation test platform.

correction of the body and DLC control loop is to change the external force vector of the body. Firstly, the attitude correction module provides the correction commands of the ship attitude, which is generally three Euler angles. And then, the corresponding external loop realizes the conversion of the Euler angle commands to the internal angular rate commands.

$$\dot{\boldsymbol{\Phi}} = K_{\Phi}\left(\boldsymbol{\Phi}_{\mathrm{c}} - \boldsymbol{\Phi}\right) \tag{55}$$

where K_{Φ} is cutoff frequency parameters of the Euler angle for updating.

The obtained Euler angular rate commands are converted to the triaxial angular rate commands by Eq. (3). Then the three-axis angular rate commands in stability coordinate is obtained by the coordinate transformation relation $\boldsymbol{T}_{\mathrm{sb}}$.

As for trajectory tracking commands, it is to give full play to the function of direct lift. The corresponding control states are $(\gamma_{\mathrm{c}}, |V|)$, the design of the outer loop should ensure that the sliding slop angle error can be transmitted directly to the surface deflection of direct lift while the ship speed is stable. We use the first-order proportional relationship to transform the dynamics of corresponding states as follow:

$$\begin{aligned} \dot{V}_{\mathrm{c}} &= K_V(V_{\mathrm{c}} - V) \\ \dot{\gamma}_{\mathrm{c}} &= K_{\gamma}(\gamma_{\mathrm{c}} - \gamma) \end{aligned} \tag{56}$$

where K_V and K_{γ} are the cut-off frequency parameters of the corresponding states.

V. SIMULATION AND ANALYSIS

The simulation will be divided into three part for analysis. The first subsection is trajectory tracking control analysis used for validation of the correction of INDI+DCL control effects in precision carrier landing. The second subsection is landing simulation with two different disturbances used for demonstrating the disturbance rejection ability of INDI+DLC control framework. The last part is the simulation of the robustness comparison between INDI and NDI baseline control law for DLC.

A. TRAJECTORY TRACKING CONTROL

The flight simulations were initialized in trim conditions at an altitude of 114m and speed of 195 m/s. As shown in Fig. 11,

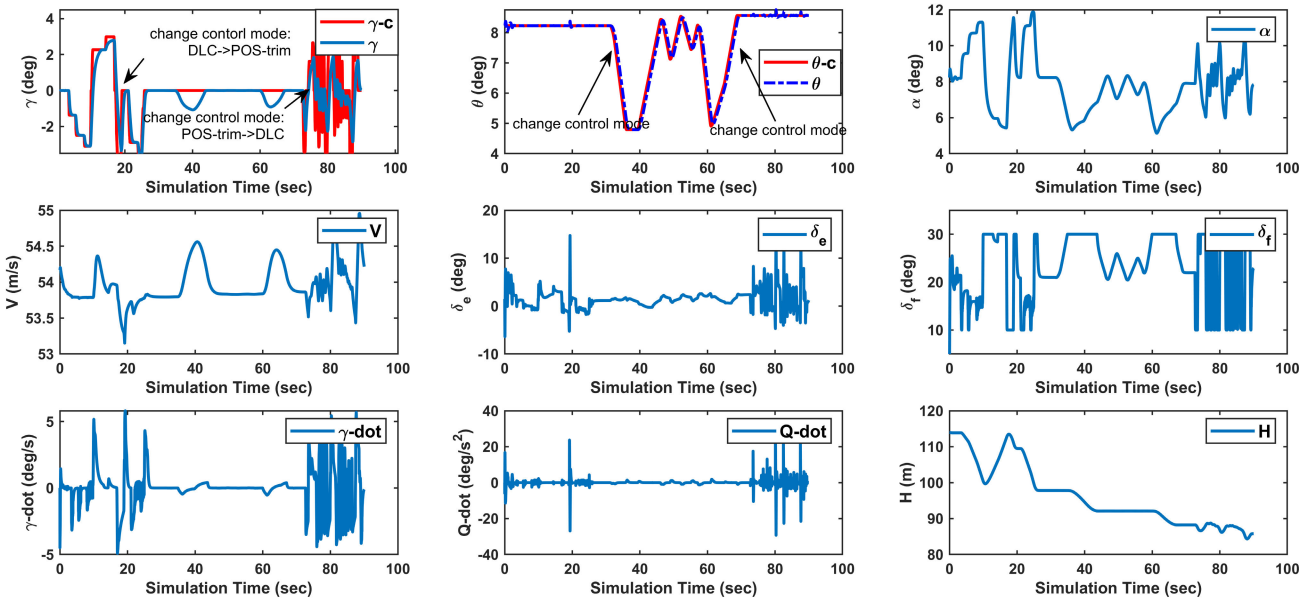

FIGURE 12. The graph of track manipulation and attitude manipulation response under increment dynamic inversion frame.

the simulation test platform mainly includes the joystick, pedal, throttle hardware input platform, Simulink dynamic model, and flight-gear simulator.

The INDI + DLC controller is applied to the full-state nonlinear carrier aircraft simulation model. Two command modules (DLC or POS_Trim) are switched through the pick of throttle platform to realize the control stick commands, which is corresponding to the trajectory tracking control command (γ_c) and attitude adjustment control command (θ_c), respectively.

The tracking histories of the controlled variables for two different command modules switched in the 100s simulation times are displayed and compared in Fig.12. In the first 20s, we use the function of longitude stick to generate DLC-trajectory command γ_c, we can see that the trajectory control variable γ follows its command γ_c without large delay and overshoot while the aircraft attitude angle θ keep still at 8° and velocity oscillate at $V \approx 54m/s$ with small amplitude of 0.5 m/s. Other response records of control surface δ_e, δ_f, attack of angle α, the derivation of landing glide angle $\gamma - dot$ and the derivation of pitch angle rate $Q - dot$, all indicate the control performance of trajectory tracking with the direct lift. During 20s to 70s, we change command module from DLC to POS_Trim, in contrast, the pitch angle is simultaneously selected to be controlled with longitudinal stick input compared with stick input indicates gliding angle. We can see that INDI control framework without using DLC to tracking flight path, the attitude of the aircraft also can be controlled with longitude stick inputs. During 70s to 100s, we switch back to DLC control module with more quick stick input. it can be seen that γ just change following the command $\gamma - c$ at the same time. Compared the response of DLC and POS_Trim modules, we can conclude the following

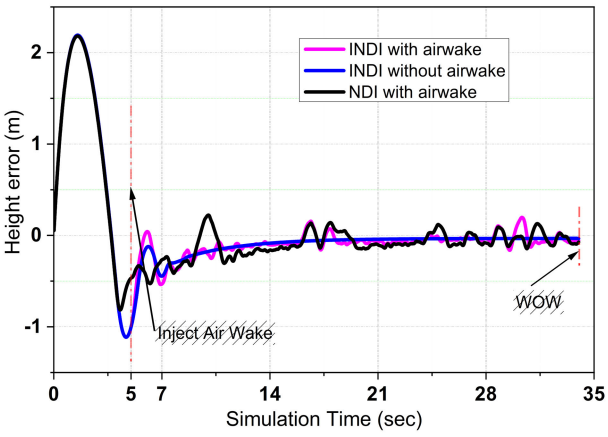

FIGURE 13. The response of height error in the condition of ship air wake.

points: (1) the direct lift control designed on the INDI framework achieves the control targets of correcting the tracking error with guaranteeing the attitude stability, by using the direct lift force generated by the direct lift surface. (2) the direct lift mode can quickly correct the altitude error introduced by pitch moment disturbances, ultimately, realize the aim of quickly tracking after the trajectory is disturbed.

B. LANDING SIMULATION ANALYSIS

1) SHIP AIR WAKE DISTURBANCES

This subsection illustrates the air-wake disturbances rejection of the designed control framework. Firstly, the aircraft is trimmed at the beginning of the aircraft gliding point ($x = -1863m, z = -114m$), the trajectory angles are as follows: $\gamma = 0°, \alpha = 8°, \gamma = -3.5°$. The aircraft gliding simulation

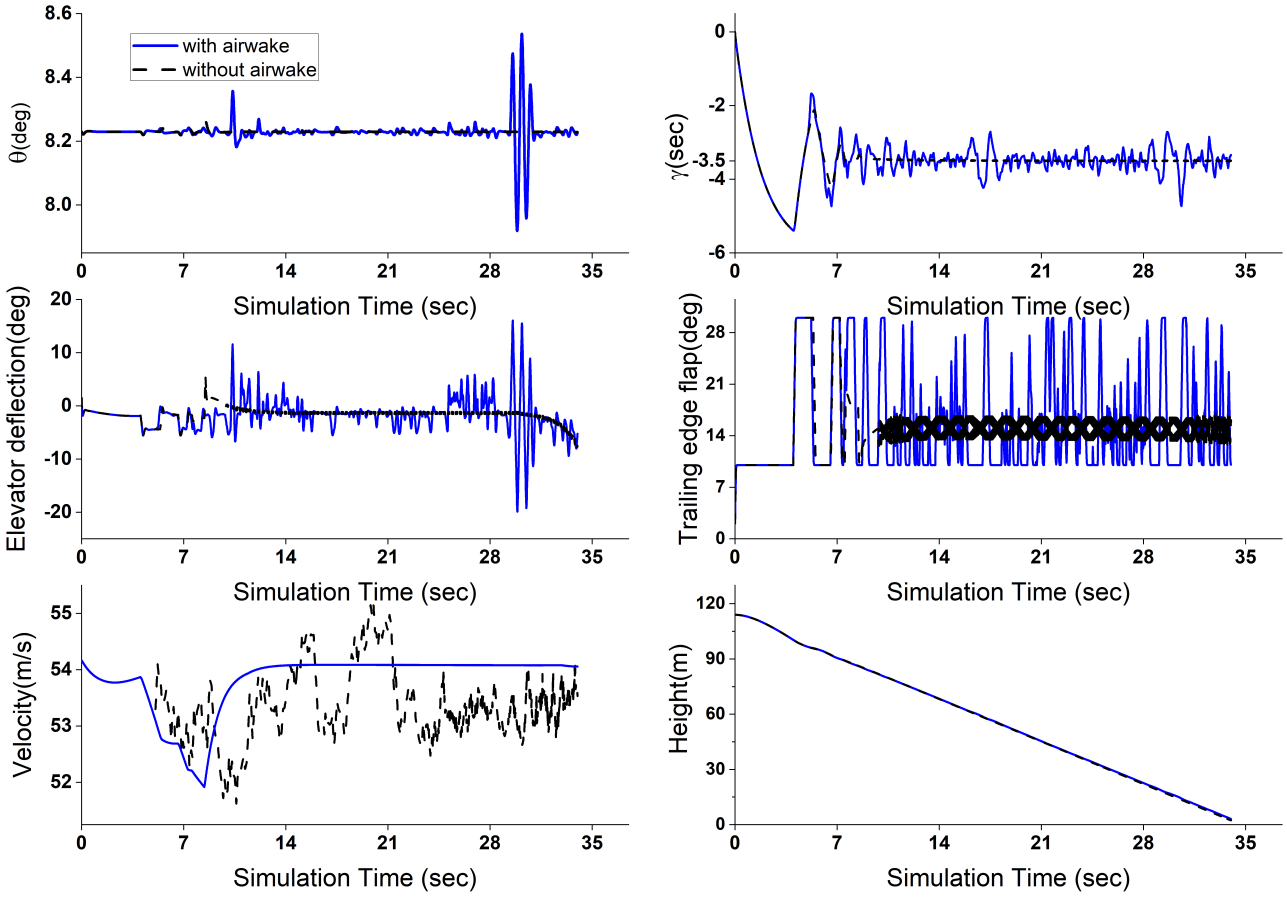

FIGURE 14. The response of states in the condition of ship air wake.

is carried out according to the expected gliding angle of the flight path. After the first 5s, the air wake disturbance is injected into the ship's landing simulation.

From Fig. 13, we can see that the carrier aircraft captures the desired glide path after the initial height adjustment. Under the influence of the air wake, the error of landing height is stable on the ideal glide path, the peak error of landing height is less than 0.5 m, and the horizontal error is less than 8.1 m, which indicates that the error is between an arresting rope (12 m).

The attitude loop's state response and the trajectory loop's primary state response during the aircraft glide simulation are illustrated in Fig. 14. We can find the following results: (1) the dip angle of the glide path is adjusted from 0° to −3.5° and remains stable; (2) After the disturbance of ship air wake, the dip angle rapidly responds to the disturbances of the vertical velocity of the ship wake, which stabilizes the ship's height in the desired glide path. Because the elevator surface deflection eliminates the pitch moment disturbances introduced by the trajectory loop correction command, the pitch angle of the attitude loop can be stable around 8.25° during the course of trajectory adjustment. The results indicate that INDI has a stronger disturbance suppression ability.

2) INITIAL ERROR DISTURBANCES

In order to further analyze the improvement of landing characteristics in the INDI+DLC control framework, the initial approach error is introduced into the simulation environment, that is, the height error (+10m, −5m) and the glide path angle error (+3°) are introduced into the landing start point.

Fig. 15 depicts that the direct lift track control law designed in NDI or INDI framework can quickly capture the desired glide path under the initial error disturbances. In addition, the response of height error in INDI control architecture is slightly worse than that in NDI control architecture. However, if the track loop of INDI control framework was replaced by the NDI control loop used for comparison, the height error response was significantly improved.

The controlled states' response showed in Fig. 16. Compared with INDI, the NDI control frame has a slightly worse ability to suppress pitch disturbances in the attitude loop when trajectory tracking is performed by direct lift force. Whereas, INDI control frame's attitude stabilization loop has a worse ability to track pitch command. Therefore, using the NDI control method in the trajectory loop and the INDI control method in the attitude loop can guarantee the DLC glide

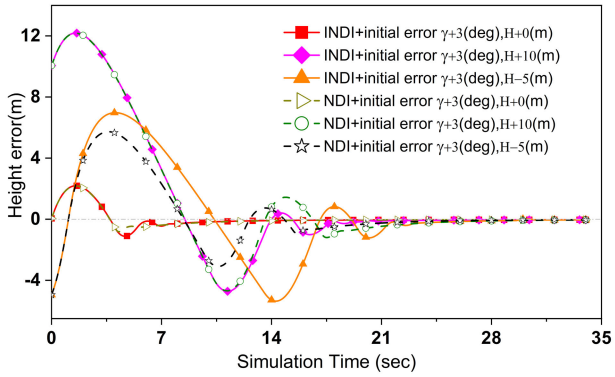

FIGURE 15. The response of height errors in the condition of initial error.

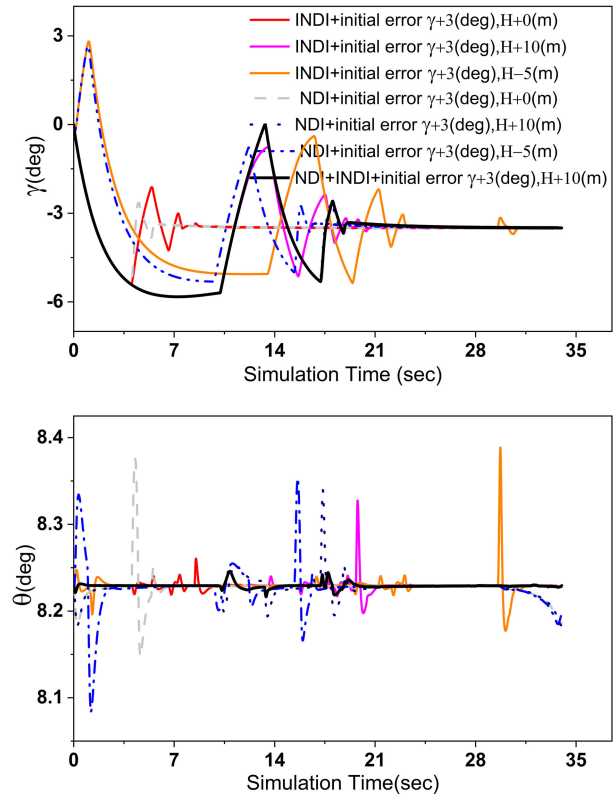

FIGURE 16. The response of states in the condition of the initial error.

path correction and the good dynamic suppression ability to the attitude disturbances.

C. ROBUST SIMULATION ANALYSIS

In order to further distinguish between INDI and NDI and DLC implemented by INDI is more robust than that implemented by NDI, the simulation was conducted at the following condition: (1) the ship wake disturbances are introduced after 5s; (2) The other control loops remain the same while the inversion forms are changed.

Fig. 17 indicates that INDI is slightly robust to external disturbances but not for the inaccuracy of the aircraft parameters. Because the dependence of the INDI control loop on

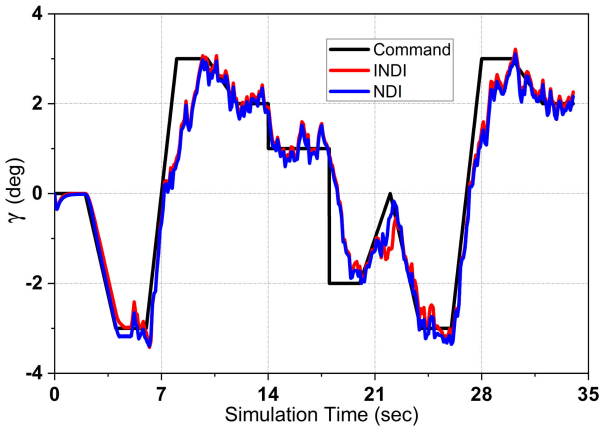

FIGURE 17. The response of gliding angle with NDI and INDI control frame.

the aircraft model is significantly reduced and only reflected on the last moment of feedback information. Even so, INDI has the same dependence on the aerodynamic model as NDI. Therefore, to analyze the INDI control architecture is more robust than NDI, the inertia parameters of the simulation model should be deliberately changed. The INDI/ NDI loop is respectively simulated 15 times, the center of gravity of the aircraft is moved backward according to a specific increment $\Delta X_{cg} = 0.3\%$ at each time. The center of gravity is changed compared with the actual value, and the static stability of the aircraft is relaxed.

The results shown in Fig. 18, cold color (black to blue) is NDI related response records, hot color (pink to red) is INDI related response records. We can see that the NDI control framework induces significant fluctuation at the 10th time compared with the previous times. It can be attributed to the inaccurate inversion feedback dynamics of the NDI attitude loop, and the inversion feedback dynamics cannot eliminate the dynamics of aircraft and then introduce errors, which results in the oscillation and divergence of the attitude loop. In contrast, the trajectory loop can still track the trajectory command under the direct lift. We can conclude that the influence of the longitudinal static stability error on the trajectory loop is less significant than that of the attitude loop. In 15 simulations, the INDI control framework, which can be seen, has more capacity to suppress disturbances of the pitch moment introduced by direct force tracking manipulation. On the other hand, it diverges later when the false center of gravity position is input compared to the NDI. The INDI control framework has better robustness than NDI with false input center of gravity position.

VI. CONCLUSION

This paper introduces DLC into the NDI/ INDI control architecture for precision carrier landing. The simulation results indicate that the NDI/INID +DLC design method can effectively restrain the disturbance effect of air wakes and initial

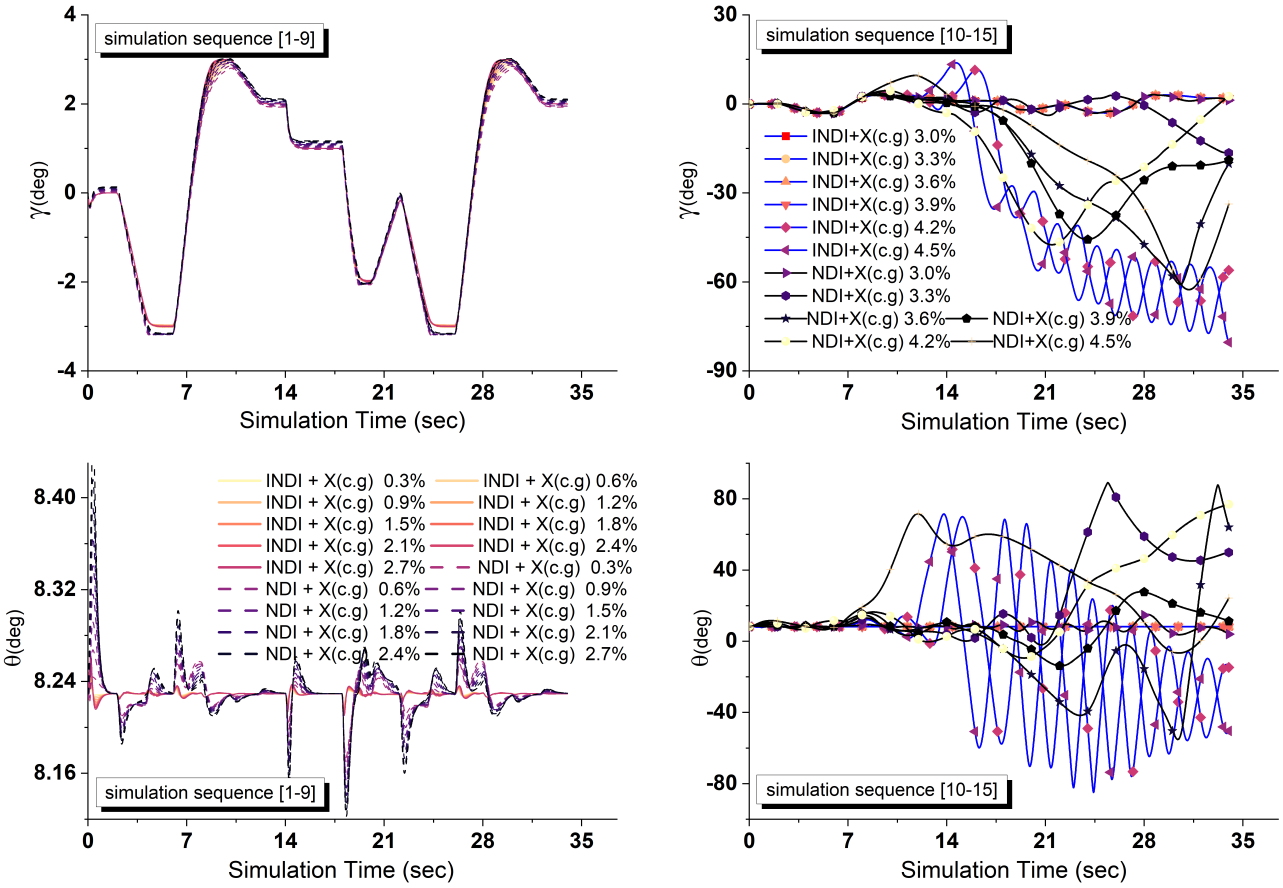

FIGURE 18. The response of attitude and trajectory states with wrong parameters of gravity position center.

altitude error on the glide path angle of carrier aircraft. The innovation of the NDI/INDI+DLC precision landing control architecture can be mainly summarized as follows:

(1) The INDI/ NDI + DLC control architecture designed in this paper has the characteristics of the full use of direct lift to improve aircraft landing quality. By using the speediness of direct lift, the ship glide path error is corrected, and the ship maneuvering complexity is reduced by using the decoupling ability of direct lift and dynamic inversion control methods. This indicates that using dynamic inversion control methodology to implement DLC is a new solution of using direct force to improve fly-by-wire aircraft performance.

(2) In this paper, considering that INDI can improve the robustness of NDI, it is proved by simulation that INDI is more robust than NDI. However, through simulation analysis of the aircraft landing, the NDI control frame is adopted in the track loop, and the INDI control frame is used in the attitude loop. The direct lift control of ship landing is realized on such combined architecture. The results indicate that it has better track correction ability and a higher ability to suppress disturbances of the attitude loop.

ACKNOWLEDGMENT

The authors greatly acknowledge the supply of the aerodynamics model of a fixed-wing carrier aircraft and simulation equipment, as well as providing timely suggestions and help on this project.

REFERENCES

[1] R. T. Gralow, J. D. Peace, III, and J. L. Shipley, "Evaluation of the direct lift control system installed in the F-8C airplane," U.S. Naval Air Test Center, Patuxent River, MD, USA, Tech. Rep. FT-51R-65(RA1300001), 1965.

[2] D. Wilkin and H. Stiles, "Optimizing the F-14 A DLC/APC system for improved glideslope performance," in *Proc. 13th Annu. Symp.*, New York, NY, USA, 1982, pp. 143–149.

[3] J. W. Denham, "Project MAGIC CARPET: Advanced controls and displays for precision carrier landings," in *Proc. 54th AIAA Aerosp. Sci. Meeting*, Jan. 2016, pp. 1–14, doi: 10.2514/6.2016-1770.

[4] W. Ellison and J. Latz, "Design and flight testing of the X-35 air data system," in *Proc. AIAA Atmos. Flight Mech. Conf. Exhibit*, Aug. 2003, p. 5319.

[5] F. Grondman, G. Looye, R. O. Kuchar, Q. P. Chu, and E.-J. Van Kampen, "Design and flight testing of incremental nonlinear dynamic inversion-based control laws for a passenger aircraft," in *Proc. AIAA Guid., Navigat., Control Conf.*, Jan. 2018, p. 385.

[6] M. D. Pavel, P. Shanthakumaran, Q. Chu, O. Stroosma, M. Wolfe, and H. Cazemier, "Incremental nonlinear dynamic inversion for the apache AH-64 helicopter control," *J. Amer. Helicopter Soc.*, vol. 65, no. 2, pp. 1–16, Apr. 2020, doi: 10.4050/JAHS.65.022006.
[7] J. Horn, "Non-linear dynamic inversion control design for rotorcraft," *Aerospace*, vol. 6, no. 3, p. 38, Mar. 2019, doi: 10.3390/aerospace6030038.
[8] S. A. Raab, J. Zhang, P. Bhardwaj, and F. Holzapfel, "Proposal of a unified control strategy for vertical take-off and landing transition aircraft configurations," in *Proc. Appl. Aerodyn. Conf.*, Jun. 2018, p. 3478, doi: 10.2514/6.2018-3478.
[9] T. Lombaerts, J. Kaneshige, S. Schuet, B. L. Aponso, K. H. Shish, and G. Hardy, "Dynamic inversion based full envelope flight control for an eVTOL vehicle using a unified framework," in *Proc. AIAA Scitech Forum*, Jan. 2020, p. 1619, doi: 10.2514/6.2020-1619.
[10] E. Safwat, W. Zhang, A. Kamel, and M. Kassem, "Robustness analysis of modified incremental nonlinear dynamic inversion for small UAVs," *Autom. Control Comput. Sci.*, vol. 54, no. 2, pp. 128–138, Mar. 2020, doi: 10.3103/S0146411620020078.
[11] S. Sun, X. Wang, Q. Chu, and C. D. Visser, "Incremental nonlinear fault-tolerant control of a quadrotor with complete loss of two opposing rotors," *IEEE Trans. Robot.*, vol. 37, no. 1, pp. 116–130, Feb. 2021, doi: 10.1109/TRO.2020.3010626.
[12] X. Wang, E.-J. van Kampen, and Q. Chu, "Quadrotor fault-tolerant incremental nonsingular terminal sliding mode control," *Aerosp. Sci. Technol.*, vol. 95, Dec. 2019, Art. no. 105514, doi: 10.1016/j.ast.2019.105514.
[13] O. Pfeifle and W. Fichter, "Cascaded incremental nonlinear dynamic inversion for three-dimensional spline-tracking with wind compensation," *J. Guid., Control, Dyn.*, vol. 44, no. 8, pp. 1–13, 2021, doi: 10.2514/1.g005785.
[14] E. J. J. Smeur, G. C. H. E. de Croon, and Q. Chu, "Cascaded incremental nonlinear dynamic inversion for MAV disturbance rejection," *Control Eng. Pract.*, vol. 73, pp. 79–90, Apr. 2018, doi: 10.1016/j.conengprac.2018.01.003.
[15] X. Wang, T. Mkhoyan, and R. De Breuker, "Nonlinear incremental control for flexible aircraft trajectory tracking and load alleviation," in *Proc. AIAA Scitech Forum*, Jan. 2021, pp. 1–19, doi: 10.2514/6.2021-0503.
[16] G. Wu, X. Meng, and F. Wang, "Improved nonlinear dynamic inversion control for a flexible air-breathing hypersonic vehicle," *Aerosp. Sci. Technol.*, vol. 78, pp. 734–743, Jul. 2018, doi: 10.1016/j.ast.2018.04.036.
[17] Z. Zhen, G. Tao, C. Yu, and Y. Xue, "A multivariable adaptive control scheme for automatic carrier landing of UAV," *Aerosp. Sci. Technol.*, vol. 92, pp. 714–721, Sep. 2019, doi: 10.1016/j.ast.2019.06.030.
[18] M. Lungu, "Auto-landing of UAVs with variable centre of mass using the backstepping and dynamic inversion control," *Aerosp. Sci. Technol.*, vol. 103, Aug. 2020, Art. no. 105912, doi: 10.1016/j.ast.2020.105912.
[19] M. Lungu, "Backstepping and dynamic inversion combined controller for auto-landing of fixed wing UAVs," *Aerosp. Sci. Technol.*, vol. 96, Jan. 2020, Art. no. 105526.
[20] S. Zhang and Q. Meng, "An anti-windup INDI fault-tolerant control scheme for flying wing aircraft with actuator faults," *ISA Trans.*, vol. 93, pp. 172–179, Oct. 2019.
[21] G. Di Francesco, E. D'Amato, and M. Mattei, "INDI control with direct lift for a tilt rotor UAV," *IFAC-PapersOnLine*, vol. 48, no. 9, pp. 156–161, 2015, doi: 10.1016/j.ifacol.2015.08.076.
[22] Y. Yan, J. Yang, C. Liu, M. Coombes, S. Li, and W.-H. Chen, "On the actuator dynamics of dynamic control allocation for a small fixed-wing UAV with direct lift control," *IEEE Trans. Control Syst. Technol.*, vol. 28, no. 3, pp. 984–991, May 2020, doi: 10.1109/TCST.2019.2945909.
[23] T. Lombaerts and G. Looye, "Design and flight testing of nonlinear autoflight control laws incorporating direct lift control," in *Advances in Aerospace Guidance, Navigation and Control*. 2013, pp. 549–568, doi: 10.1007/978-3-642-38253-6_32.
[24] F. Luo, J. Zhang, and B. Wang, "Research on air wake rejection based on direct lift control and nonlinear dynamic inversion control method," *Acta Aeronaut. Astronaut. Sinica*, vol. 42, no. 7, p. 124770, 2021, doi: 10.7527/S1000-6893.2020.24770.
[25] D. J. Moorhouse and R. J. Woodcock, "Background information and user guide for MIL-F-8785C, military specification-flying qualities of piloted airplanes," Air Force Wright Aeronaut. Lab., Wright-Patterson AFB, OH, USA, Tech. Rep. AFWAL-TR 81-3109, 1982.
[26] X. Wang, E.-J. van Kampen, Q. Chu, and P. Lu, "Stability analysis for incremental nonlinear dynamic inversion control," *J. Guid., Control, Dyn.*, vol. 42, no. 5, pp. 1116–1129, May 2019.
[27] F. Luo, J. Zhang, and B. Jiang, "Robustness analysis of two advanced flight control laws: NDI and INDI," in *Proc. 5th China Aeronaut. Sci. Technol. Conf.*, 2022, pp. 660–668.
[28] A. L. Fradkov, I. V. Miroshnik, and V. O. Nikiforov, *Nonlinear and Adaptive Control of Complex Systems*. Dordrecht, The Netherlands: Springer, 1999, doi: 10.1007/978-94-015-9261-1.
[29] S. Juliana, Q. P. Chu, J. A. Mulder, and T. J. van Baten, "The analytical derivation of nonlinear dynamic inversion control for parametric uncertain system," in *Proc. AIAA Guid., Navigat., Control Conf. Exhibit*, vol. 1, Aug. 2005, pp. 342–355, doi: 10.2514/6.2005-5849.
[30] C. Ahn, H. Kim, and Y. Kim, "Adaptive sliding mode control for non-affine nonlinear vehicle systems," in *Proc. AIAA Guid., Navigat. Control Conf. Exhibit*, vol. 2, Aug. 2007, pp. 1741–1757, doi: 10.2514/6.2007-6506.

FEI LUO received the B.S. degree in weapon system engineering from the Beijing Institute of Technology, in 2018, and the M.S. degree in system engineering from the China Academy of Aeronautics, in 2021. He became an Assistant Engineer with the First Aircraft Design and Research Institute, Aviation Industry Corporation of China, Ltd., Xi'an, China. His main research interest includes carrier-based aircraft landing control.

JUNHONG ZHANG is currently pursuing the Ph.D. degree with Northwestern Polytechnical University, China. Since 2005, he has been engaged in developing an aircraft flight control system with the First Aircraft Design and Research Institute, Aviation Industry Corporation of China, Ltd., Xi'an, China. As the Chief Designer of the flight control system of an aircraft, he presided over the development and flight test verification of the system. He is the Master Supervisor with the China Aviation Research Institute and a particular Technical Expert of Aviation Industry Corporation. His expertise covers aircraft-flight-control system architecture design, flight control law design, and airborne software architecture design.

PENGFEI LYU received the B.E. degree in aircraft design and engineering from Beihang University, Beijing, China, in 2008, the MA.Eng. degree in aircraft design from Chinese Aeronautical Establishment, China, in 2014, and the advanced master's degree in aeronautical engineering from ISAE-SUPAERO University, France, in 2017. He works with the First Aircraft Design and Research Institute, Aviation Industry Corporation of China, Ltd., Xi'an, China.

ZHENGBAO LIU (Member, IEEE) received the B.S. and M.S. degrees from Northwestern Polytechnical University, Xi'an, China, in 2004, and the Ph.D. degree from the University of Tsukuba, Japan, in 2009.

From 2009 to 2010, he was a Visiting Scholar at the University of Tokyo, Japan. From 2010 to 2016, he was an Associate Professor at Northwestern Polytechnical University. His research interests include autonomous flight control, autonomous obstacle avoidance and formation, and aircraft fault diagnosis and fault-tolerant control. He was an Associate Editor of IEEE Access Journal of the American Society of Electrical and Electronics Engineers, a Senior Member of the IEEE Aerospace Electronics Society, and the Chinese Society of Aeronautics. He is an Evaluation Expert of the Science and Technology Committee of the Military Commission, the Equipment Development Department of the Military Commission, and the Ministry of Education Degree Center, in China. He also served as the aircraft-model development Review Expert for the AVIC First Aircraft Design Institute. He served for the IEEE Transactions on Neural Network and Learning Systems, IEEE Transactions on Aerospace and Electronic Systems, IEEE Transactions on Cybernetics, IEEE Transactions on Industrial Electronics, and other journals.

WEI TANG (Member, IEEE) received the B.S. degree in mechanical engineering, the M.S. degree in mechatronics, and the Ph.D. degree in automation engineering from Northwestern Polytechnical University, Xi'an, China, in 2000, 2003, and 2006, respectively.

From 2006 to 2009, he was a Research Assistant at the Automation School, Northwestern Polytechnical University, where he has been an Associate Professor, since 2009. From 2009 to 2010, he was a Visiting Scholar at the Department of Electronics and Computer, Newcastle University, Australia. His research interests include vibration control, robots and intelligent systems, and aero-engine control.

Dr. Tang was a recipient of the Second Prize of National Defense Technology Invention, in 2015, and the Second Prize of National Defense Science and Technology Progress Award, in 2009. He serves as a Reviewer for the journals, such as *Acta Aeronautica*, *Shock and Vibration*, *System Engineering Theory and Practice*, and other journals.